

A TRIDENT SCHOLAR PROJECT REPORT

NO. 276

THE USE OF MEMS TO DETECT VIBRATIONS ASSOCIATED WITH
ABNORMAL SCROLL COMPRESSOR OPERATION



UNITED STATES NAVAL ACADEMY
ANNAPOLIS, MARYLAND

This document has been approved for public
release and sale; its distribution is unlimited.

20010717 128

USNA-1531-2

REPORT DOCUMENTATION PAGE

Form Approved
OMB No. 074-0188

Public reporting burden for this collection of information is estimated to average 1 hour per response, including the time for reviewing instructions, searching existing data sources, gathering and maintaining the data needed, and completing and reviewing the collection of information. Send comments regarding this burden estimate or any other aspect of the collection of information, including suggestions for reducing this burden to Washington Headquarters Services, Directorate for Information Operations and Reports, 1215 Jefferson Davis Highway, Suite 1204, Arlington, VA 22202-4302, and to the Office of Management and Budget, Paperwork Reduction Project (0704-0188), Washington, DC 20503.

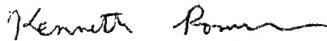
1. AGENCY USE ONLY (Leave blank)		2. REPORT DATE 3 May 2000		3. REPORT TYPE AND DATE COVERED	
4. TITLE AND SUBTITLE The use of MEMs to detect vibrations associated with abnormal scroll compressor operation				5. FUNDING NUMBERS	
6. AUTHOR(S) Roman, Kenneth M.					
7. PERFORMING ORGANIZATION NAME(S) AND ADDRESS(ES) U.S. Naval Academy Annapolis, MD				8. PERFORMING ORGANIZATION REPORT NUMBER USNA Trident Scholar project report no. 276 (2000)	
9. SPONSORING/MONITORING AGENCY NAME(S) AND ADDRESS(ES)				10. SPONSORING/MONITORING AGENCY REPORT NUMBER	
11. SUPPLEMENTARY NOTES Accepted by the U.S. Trident Scholar Committee					
12a. DISTRIBUTION/AVAILABILITY STATEMENT This document has been approved for public release; its distribution is UNLIMITED.					12b. DISTRIBUTION CODE
13. ABSTRACT: MicroElectroMechanical Systems (MEMs) are silicon microchips that have both electrical and mechanical components. The mechanical components convert mechanical signals to electrical signals for further processing. The application of MEMs technology to compressors is being explored by the National Institute of Standards and Technology for the Copeland Corporation, a manufacturer of scroll compressors. This project investigates the use of MEMs to detect vibrations associated with abnormal scroll compressor operation. The mechanical component on the MEMs is a vibration sensitive micro-cantilever beam with an encapsulated piezoresistor. Results for circuit operability are presented and piezoresistive vibration sensitivities of various length cantilevers are determined. A model for the vibration sensitivity is developed using the dimensions and properties of the piezoresistive cantilevers. A testing technique is developed that can be used to determine sensitivity for any cantilever geometry. The vibration sensitivity model and experimentation are used to identify the most sensitive cantilever design. The value of the piezoresistive coefficient is shown to be 190. This study shows that sensitivity increases with beam length and frequency of vibration. The best length cantilever is 1.6 mm. A shorter length may be acceptable if a built-on amplifier is used.					
14. SUBJECT TERMS cantilever, MEMs, piezoresistive sensor, sensitivity, vibration sensor				15. NUMBER OF PAGES	
				16. PRICE CODE	
17. SECURITY CLASSIFICATION OF REPORT		18. SECURITY CLASSIFICATION OF THIS PAGE		19. SECURITY CLASSIFICATION OF ABSTRACT	
20. LIMITATION OF ABSTRACT					

U.S.N.A. — Trident Scholar project report; no. 276 (2000)

**THE USE OF MEMS TO DETECT VIBRATIONS ASSOCIATED WITH
ABNORMAL SCROLL COMPRESSOR OPERATION**

by

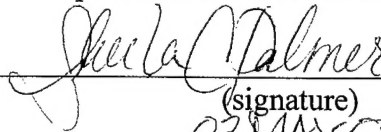
Midshipman Kenneth M. Roman, Class of 2000
United States Naval Academy
Annapolis, Maryland



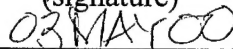
(signature)

Certification of Advisers Approval

Assistant Professor Sheila C. Palmer
Department of Mechanical Engineering

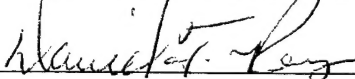


(signature)

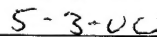


(date)

LCDR Daniel T. Ray, USNR
Department of Mechanical Engineering



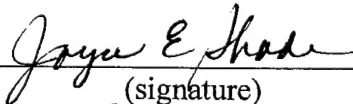
(signature)



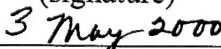
(date)

Acceptance for the Trident Scholar committee

Professor Joyce E. Shade
Chair, Trident Scholar Committee



(signature)



(date)

USNA-1531-2

Abstract:

MicroElectroMechanical Systems (MEMS) are silicon microchips that have both electrical and mechanical components. The mechanical components convert mechanical signals to electrical signals for further processing. The application of MEMS technology to compressors is being explored by the National Institute of Standards and Technology for the Copeland Corporation, a manufacturer of scroll compressors. This project investigates the use of MEMS to detect vibrations associated with abnormal scroll compressor operation. The mechanical component on the MEMS is a vibration sensitive micro-cantilever beam with an encapsulated piezoresistor.

Results for circuit operability are presented and piezoresistive vibration sensitivities of various length cantilevers are determined. A model for the vibration sensitivity is developed using the dimensions and properties of the piezoresistive cantilevers. A testing technique is developed that can be used to determine sensitivity for any cantilever geometry. The vibration sensitivity model and experimentation are used to identify the most sensitive cantilever design.

The value of the piezoresistive coefficient is shown to be 190. This study shows that sensitivity increases with beam length and frequency of vibration. The best length cantilever is 1.6 mm. A shorter length may be acceptable if a built-on amplifier is used.

Key words: cantilever, MEMS, piezoresistive sensor, sensitivity, vibration sensor

Nomenclature:

A	Segment of the beam with piezoresistor
A_z	Cross-sectional area of beam (m^2)
B	Segment of the beam without piezoresistor
c	Length of segment A (m)
E	Elasticity (N/m^2)
EI	Flexural rigidity ($N\ m^2$)
G	Gain of amplifier
h	Distance from neutral plane of piezoresistor to neutral plane of segment A (m)
H	Height (m)
I	Moment of inertia (m^4)
L	Length of (m)
m	Mass per unit length (kg/m)
R	Resistance of the piezoresistor (ohm)
s	Arc distance (m)
S	Piezoresistive sensitivity ($1/m$)
t	Time (s)
u	Non-dimensionalized length (x/L)
V	Voltage (V)
w	Width (m)
y	Displacement in the y-direction (m)
Z	Piezoresistive coefficient

Greek

n_0	Amplitude of shaker table (y-direction) (m)
ρ	Density (kg/m^3)
ω	Natural angular frequency of the shaker table (radians)
α	Non-dimensionalized length (c/L)
Δ	Change (final minus initial)
ν	Poisson's ratio

Subscripts:

a	Positive voltage output of Wheatstone bridge
b	Negative voltage output of Wheatstone bridge
A	Segment A
B	Segment B
max	Maximum
min	Minimum
NPP	Neutral plane of piezoresistor
NPB	Neutral plane of beam
n	1,2,3,4
o	Voltage source or initial value

Bridge Descriptions:

Bridge1	Wheatstone bridge located in upper center of chip with built-on Amp
Bridge2	Wheatstone bridge located in upper right corner of chip
Bridge3	Wheatstone bridge located in upper left corner of chip
Bridge4	Wheatstone bridge located at bottom of chip

Package Descriptions:

Package1	Bridge3 and external amplifier
Package2	Bridge4 and external amplifier

List of Figures:

Figure 1	Schematic of Prototype MEMS	34
Figure 2	Close Up View of a Typical Cantilever	35
Figure 3	Wheatstone Bridge Details	36
Figure 4	Side-view of a Typical cantilever	37
Figure 5	Cross Section of Segment A of a Typical Cantilever	37
Figure 6	Local Radius of Curvature of a Typical Cantilever	38
Figure 7	Circuitry to Test Operability of Built-on Amplifier for Bridge1	39
Figure 8	Built-on Amplifier Data	40
Figure 9	External Amplifier Characteristics	41
Figure 10	MEMS Testing Equipment Set-up	42
Figure 11	Typical MEMS Package in a Cerdip Die Well	43
Figure 12	Package1 (Bridge3 with an External Amplifier)	44
Figure 13	Package2 (Bridge4 with an External Amplifier)	45
Figure 14	Wire Bonding Machine	46
Figure 15	Physical Layers of Beam	47
Figure 16	Gain of External Amplifier on Shaker Table	48
Figure 17	Oscilloscope Reading of Voltages from Shaker Table and Package2	49
Figure 18	Sensitivity of Cantilevers	50
Figure 19	Deflection of Cantilevers	50
Figure 20	Noise Reading on Oscilloscope	51
Figure 21	Noise Pick-up	52
Figure 22	Voltage from Wheatstone Bridges Compared to Noise	53

Table of Contents:

Abstract	2
Nomenclature	3
List of Figures	5
1. Introduction	8
2. Background	9
2.1 General Overview of MEMS	9
2.2 Overview of Prior Work on MEMS at NIST	11
2.2.1. Selection of a Vibration Sensor System	12
2.2.2. Design of the MEMS Prototype	12
2.2.3. Manufacturing of the Prototype Chip	14
3. Theory	15
3.1. Cantilever Model	15
3.1.1. Differential Equations of Motion for a Cantilever Beam	15
3.2. Strain in Piezoresistive Layer	18
3.3. Instantaneous Resistance of Cantilever	18
3.4. Piezoresistive Sensitivity	19
3.5. Determination of the Piezoresistive Coefficient	19
4. Experimentation	21
4.1. Preliminary Tests	21
4.2. Selection of External Amplifier	22
4.3. Setup of Tests with MEMS and External Amplifier	23
4.3.1. Preparation Process of MEMS Package	23
5. Determination of Beam Properties	24
5.1. Cantilever Model	24
5.2. Determination of Flexural Rigidity and Mass per Unit Length	25
5.2.1. Location of Neutral Planes	26

6. Results/Discussion	27
6.1. Gain of the External Amplifier	27
6.2. Piezoresistive Sensitivity	27
6.3. Best Design Length of Cantilever	29
6.4. Effects of Noise on Experimentation	30
7. Conclusion/Recommendations	31
8. References	32
9. Figures	34
Appendix A: Equations of Motion for Cantilever Used in Project	54
Appendix B: Determination of Strain in Piezoresistive Layer	58
Appendix C: Determination of Instantaneous Resistance in Terms of Piezoresistive Sensitivity	61
Appendix D: Relating the Piezoresistive Sensitivity to Experimental Results	64
Appendix E: Determination of Beam Properties	68
Appendix F: Calculation of Distance, h , Between NPP and NPB	73
Appendix G: Sample Calculation of Z for Package1	74
Appendix H: Sample Calculation of Piezoresistive Sensitivity	75
Appendix I: Sample Calculation of Deflection	76

1. Introduction:

MicroElectroMechanical Systems (MEMS) take advantage of the powerful capabilities of computers and enhance their integration with machinery. MEMS are silicon microchips that have electrical and mechanical components. MEMS process information gathered from these components. MEMS are linked to computers and can be used to monitor machines on a detailed level providing for an accurate and timely response to changes in operating conditions. Today's technological society has an increasing need for devices which bridge the gap between computers and machinery.

MEMS in the current study are used to detect excessive vibration in heating, ventilation, and air conditioning (HVAC) equipment so that equipment can be shut off before it, or the systems connected to it, are damaged. MEMS technology applied to scroll compressors is being explored by the National Institute of Standards and Technology for the Copeland Corporation. The sensor used in this project is a vibration sensor that includes a vibration-sensitive cantilever with an encapsulated piezoresistor. This vibration sensor relies on the piezoresistive effect, a change in resistance when strain is applied.

The first objective of this project include testing of a MEMS prototype chip to determine the operability of circuit structures. The MEMS circuit structures include Wheatstone bridges and amplifiers. The second objective is to determine sensitivities of the cantilevers. The sensitivities of the cantilevers are determined by a combination of theory and experimentation. A theoretical vibration sensitivity model, developed from the equations of motion and beam properties, is used with experimental results to determine a piezoresistive sensitivity coefficient. The piezoresistive sensitivity coefficient is then used to calculate the piezoresistive vibration sensitivities of cantilevers.

2. Background:

The background contains a general overview of MEMS, including classifications and various definitions of sensitivities. In addition, previous work at NIST is discussed.

2.1 General Overview of MEMS:

MEMS have evolved from devices which push the limits of technology to components used in a variety of commercial and industrial applications. The spread of MEMS in practical commercial use results from lower fabrication costs due to advances in microelectronics. Silicon is typically used as a fabrication material due to its favorable mechanical and electrical properties. Silicon and photolithography allow for the manufacturing of mechanical components of small size and with tight tolerances.

An advance in MEMS technology is the use of complementary metal oxide (CMOS) integrated circuit (IC) chips. These MEMS are inexpensive and reliable systems where signal processing is provided by micro-sensors with on-chip circuitry. On-chip circuitry enhances sensor performance and electromagnetic system compatibility by reducing noise [Baltes, 1993]. The cost of MEMS is lower than a device with the circuitry and sensor separate because the sensor and circuitry are manufactured in a single process.

The uses of MEMS in industry include applications in the automotive industry, medical field, process control, and consumer products. The automotive industry is one of the leading users of MEMS and have applications such as pressure sensors that gauge air intake of engines and as sensors in air bags. Today automotive manufacturers purchase 41% of all the MEMS sensors [Paula, 1996]. A second large user of MEMS is the medical field. MEMS are found in infusion pumps, respirators, and kidney dialysis machines. MEMS are also used in process controls as accelerometers and gyroscopes. MEMS in the form of accelerometers and gyroscopes are used to control guidance and anti-lock brake systems. A widely used consumer product that utilizes MEMS are printers where MEMS are used as jet nozzles.

MEMS may be classified as either actuators or sensors. Sensors are non-invasive while actuators modify the environment. Sensors may be further divided into the following categories: piezoresistive, capacitive, piezoelectric, optical, and vibration (resonant and

acceleration). Many sensors combine two or more of these categories. Piezoresistive sensors exhibit a change in resistance when a strain is applied and can be made by encapsulating piezoresistive material in silicon dioxide in order to relate the mechanical properties to electrical ones. Capacitive sensors rely on the motion of the sensor or a charge passing through the sensor to change the capacitance of the sensor. In piezoelectric sensors, a charge is induced when a force is applied to the piezoelectric material. Optical sensors rely on the reflective properties of the material in the MEMS, e.g., aluminum and silicon. A type of vibration sensor is the accelerometer. An accelerometer is a thin beam with a mass suspended from it that causes the beam to bend. The displacement of the mass is transferred to the beam causing strain. A second type of vibration sensor is a vibration resonant sensors. They come in three forms: beams, bridges, and diaphragms. These structures are driven to oscillate at their resonant frequency. Changes in resonant frequency are typically monitored through the use of encapsulated piezoresistors or optical techniques.

Vibration sensors usually fall into two general categories: resonant sensors and accelerometers. The use of beams as resonant sensors is popular because the resonant frequency of a beam is related to its length. Another use of a resonant sensor is as a force sensor where an applied force results in forces at the ends of a vibrating beam which change the resonant frequency of the beam. The use of a resonant sensor is not useful in this project because the vibration frequencies of interest are not within the beam's natural frequency range.

The sensor used in this project falls into the category of a vibration sensor. It is an accelerometer used to detect vibrations. This project includes the vibration of a cantilever containing a piezoresistor.

One performance parameter of vibration sensors is the sensitivity. Van Mullem et al. [1991] define two forms of sensitivity for resonant sensors: absolute and full-scale. The sensor used is a resonant bridge where a force can be applied to change the natural frequency of the bridge. The absolute sensitivity is the slope of the force versus frequency curve at $F=0$ and the full-scale sensitivity is the ratio of the total frequency swing to the total force range. If the sensor behaves linearly over the full force range, the absolute and

full-scale sensitivities are the same.

Sensitivity, defined by Petersen [1982], is the change in voltage divided by the acceleration of the sensor and is useful for a vibration sensor. The sensor that Petersen describes is a capacitive sensor in which voltage and acceleration are related to capacitance. This sensitivity can also be related to any beam that is accelerated, i.e., vibrated, and creates a voltage. In this case the voltage would be created by a piezoelectric or piezoresistive component.

Su et al. [1999] relate deflection to a resistance or voltage. They describe a deflection sensitivity which is defined as a ratio of the change of cantilever resistance to the end deflection (maximum deflection at the free end) of the cantilever. The sensitivity is used to describe a vibration sensor that has a cantilever with an encapsulated piezoresistor. Su's sensitivity is different from Petersen's, which related a voltage to acceleration. The sensitivities are related because acceleration is the second derivative of deflection.

Brand [1994] gives a piezoresistive sensitivity that relates the change in resistance of a piezoresistive cantilever to the amplitude of a sinusoidal vibration driving the fixed end of a cantilever beam. This sensitivity can be related to Su's and Petersen's sensitivities because deflection and acceleration are both functions of the amplitude driving the cantilever.

Most vibration sensors contain piezoelectric or piezoresistive material. Chiriac et al. [1999] describe the strain sensitivity for materials which have electromechanical properties. The strain sensitivity is evaluated by using a dimensionless parameter, k , which is called the gauge factor. The gauge factor is the ratio of the normalized change in resistance over strain. A large gauge factor is preferred to give a large change in resistance for a given strain.

2.2 Overview of Prior Work on MEMS at NIST:

This section provides a summary of the vibration sensor work done at NIST prior to the present study. The primary goal of the NIST work is to develop a vibration sensor system that can be integrated with commercial scroll compressors to detect damaging

operating conditions. Eventually the vibration sensor system may be refined so that it can detect specific compressor problems such as bearing failure, low lubricant levels, or even improper lubricants [Didion, 1998]. Once the sensor system is developed for commercial compressor's it may also be used in other HVAC equipment. NIST researchers in conjunction with Copeland Corporation developed criteria for the vibration sensor systems. These criteria are that the system must be:

1. mass produced at a low cost, adding less than three dollars to the cost of the compressor,
2. calibration-free, and
3. durable and sensitive enough for compressor operating conditions.

2.2.1. Selection of a Vibration Sensor System:

The method of production of a vibration sensor system is an important factor in meeting the low-cost criterion. One way to minimize cost is to have both sensor and circuitry integrated on one chip. The number of processing steps must be low to ensure cost-effective development. MEMS can be produced at low cost.

The second criterion is that the sensor system must be calibration-free. A mechanical component that is calibration-free is a cantilever. The cantilever is then integrated with circuitry on the MEMS chip.

The third criterion is that the sensor must be durable enough to withstand compressor operating conditions. Experimentation must be done to see if this criterion can be satisfied.

2.2.2. Design of the MEMS Prototype:

A prototype MEMS, a complimentary metal oxide sensor(CMOS) integrated circuit, was designed for the Building and Fire Research Laboratory (BFRL) at NIST by Sequoyah Technology, LLC, in consultation with the NIST Semiconductor Electronics Division. Figure 1 is a schematic of the prototype and shows arrangement of circuitry and mechanical components.

The prototype contains 31 vibration sensitive cantilevers. The cantilevers are silicon oxide encapsulating polysilicon piezoresistors. Each cantilever is 25 μm wide. There are four different lengths for the cantilevers, 0.1, 0.4, 0.8, and 1.6 mm. The 0.1 mm cantilever is a reference cantilever and all other cantilevers are sensor cantilevers. There are eight reference cantilevers, nine 0.4 mm cantilevers, nine 0.8 mm cantilevers, and five 1.6 mm cantilevers. Detail of a single cantilever is seen in Figure 2. The transparent material in the cantilever is silicon oxide. The encapsulated piezoresistor is the "U" shaped material in the silicon oxide. Along both the sides of the cantilever, pits created by an etching process are visible.

The prototype was designed to allow testing of circuit elements as well as cantilever durability and sensitivity by providing various test structures on the chip. There are seventeen cantilevers for durability testing purposes along the bottom and left side of the chip which are outlined in yellow in Figure 1. The cantilever base cross sections vary to examine the effect of shape on durability. The cantilevers have different combinations of fixed corners to determine the sensitivity to stress concentrations.

There are multiple circuit structures contained on the prototype chip. Bridge1, outlined in red on Figure 1, contains a differential amplifier that is connected to the output of a Wheatstone bridge, composed of two 0.4 mm cantilevers and two reference cantilevers. Detail of a typical Wheatstone bridge is seen in Figures 3. A second Wheatstone bridge, Bridge2, is outlined in blue on Figure 1. Bridge2 contains the same length cantilevers as Bridge1. Bridge2 does not include a differential amplifier. Bridge3, outlined in green on Figure 1, contains two 0.8 mm cantilevers and two reference cantilevers. Bridge4, outlined in orange on Figure 1, contains two 0.8 mm cantilevers and two 0.4 mm cantilevers. In order to create the separate cantilevers for Bridge4, circuitry had to be cut with a laser.

2.3. Manufacturing of the Prototype Chip:

The production of the MEMS includes a prototyping phase where the chip design is submitted to a commercial integrated circuit (IC) foundry. The foundry then produces the prototype as part of a multiple project wafer. After production by the IC foundry, a single step etching process at NIST frees sensor structures on the chip to provide an operational vibration-sensor system.

One of two post process etching techniques are used. The etching is done with an anisotropic silicon-etching solution or through the use of Xenon Difluoride, XeF_2 , gas. The use of XeF_2 gas is the best choice of the two etching techniques to free the cantilevers because surface tension is created when the liquid etching solution dries on the cantilevers breaking them. A detailed description of the XeF_2 etching process is found in Section 4.3.1 [Geist, 1998].

This project concentrates on the theory and experimentation for testing the prototype MEMS described above.

3. Theory:

A sensitivity model was developed for the MEMS cantilevers shown on the chip in Figure 1. A piezoresistor is encapsulated inside a portion of the cantilever. When the cantilever beam is deflected, the piezoresistor experiences a change in resistance which can be used to determine the piezoresistive sensitivity. The resistance of the piezoresistor depends on the strain in the piezoresistor which is a function of the slope of the beam. The equations of motion and beam properties are used to determine the deflection which, when differentiated, gives the slope and, subsequently, the strain. Strain and resistance are then related to sensitivity. In the following sections development of expressions for deflection, slope, strain, resistance, and piezoresistive sensitivity are developed.

3.1. Cantilever Model:

Figure 4 provides the side-view of a vibration sensitive cantilever. The cantilever is fixed at $x=0$ and has two segments. Segment A extends from $x=0$ to $x=c$ and contains a piezoresistor, and segment B extends from $x=c$ to $x=L$ with no piezoresistor. Segment B provides additional mass on the free end of the cantilever to provide greater deflection of the beam. The cross-sectional view of segment A is seen in Figure 5. The cross-section of segment B is the same as that for segment A except segment B contains no piezoresistor. Due to the different compositions, the properties of the segments are different.

3.1.1. Differential Equations of Motion for a Cantilever Beam:

For a beam with a cross-sectional area, A_z , the differential equation of motion is described by Euler's equation for beams [Thomson, 1998]:

$$\frac{\partial^2 y(x,t) \rho(y,z) A_z}{\partial t^2 EI(x)} + \frac{\partial^4 y(x,t)}{\partial x^4} = 0 \quad (3-1)$$

The equation assumes that the beam thickness (H) is small relative to the beam length (L), i.e., $H \ll L$, and that the geometry of the beam is uniform. In addition, the properties of the individual beam components must be homogeneous, isotropic, and within elastic limits.

Finally, the y-z plane sections must remain planar. The following development was based on Geist [1997].

For a beam of two different segments, Equation 3-1 must be developed for each segment of the beam. Continuity conditions are applied at $x=c$ to determine the overall equation of motion. Since the relationship between the length of the piezoresistor and the length of the cantilever beam is of primary importance, the x-direction in the equation of motion is normalized with respect to the beam length by letting $u=x/L$. This yields:

$$\frac{\partial^2 y}{\partial t^2} = -\frac{1}{K^2} \frac{\partial^4 y}{\partial u^4} \quad (3-2)$$

where

$$K^2 = \frac{mL^4}{EI} \quad (3-3)$$

The boundary and continuity conditions for Equation 3-2 are given below. The displacement of the fixed end of the cantilever is determined from the amplitude, y_o , and the frequency, ω , of the shaker table:

$$y_A(0, t) = y_o \sin(\omega t) \quad (3-4)$$

The slope at the fixed end of the cantilever is zero and is given by:

$$\frac{\partial y_A(0, t)}{\partial u} = 0 \quad (3-5)$$

The moment and shear force at the free end of the cantilever are zero and are given by Equations 3-6 and 3-7, respectively:

$$\frac{\partial^2 y_B(1, t)}{\partial u^2} = 0 \quad (3-6)$$

$$\frac{\partial^3 y_B(1, t)}{\partial u^3} = 0 \quad (3-7)$$

The deflection, slope, moment, and shear at $x=c$, i.e., $u=c/L=\alpha$, must be the same for segments A and B:

$$y_A(\alpha, t) = y_B(\alpha, t) \quad (\text{deflection}) \quad (3-8)$$

$$\frac{\partial y_A(\alpha, t)}{\partial u} = \frac{\partial y_B(\alpha, t)}{\partial u} \quad (\text{slope}) \quad (3-9)$$

$$(EI)_A \frac{\partial^2 y_A(\alpha, t)}{\partial u^2} = (EI)_B \frac{\partial^2 y_B(\alpha, t)}{\partial u^2} \quad (\text{moment}) \quad (3-10)$$

$$(EI)_A \frac{\partial^3 y_A(\alpha, t)}{\partial u^3} = (EI)_B \frac{\partial^3 y_B(\alpha, t)}{\partial u^3} \quad (\text{shear}) \quad (3-11)$$

Using separation of variables, the assumed form of the solution for the equation of motion is [Geist, 1997]:

$$y(u, t) = y_o \sin(\omega t) \left[1 + \frac{K^2 \omega^2 v(u)}{24} \right] \quad (3-12)$$

where [Riley, 1989]

$$v(u) = 6Cu^2 - 4Du^3 + u^4 \quad (3-13)$$

which represents the deflection of a cantilever under a uniform load when C and D are unity. The parameters C and D must be determined for each segment of the beam by applying the boundary and continuity conditions found in Equations 3-4 through 3-11 to Equation 3-12. The details of the solution of the equation of motion are found in Appendix A. The parameters C and D for segment B are expected and shown to be one because segment B is made of a single material while. Using the parameters determined for

segment A, the expression for the deflection of segment A of the beam at $u=\alpha$ is:

$$y(\alpha, t) = y_o \sin(\omega t) \left[1 + \frac{L^4 \omega^2 [2m_B (\alpha^2 - \alpha^3) + 3m_A \alpha^4]}{24(EI)_A} \right] \quad (3-14)$$

3.2. Strain in Piezoresistive Layer:

The resistance in the piezoresistive layer is related to the strain of the piezoresistor. Strain is the change in length divided by the original length. To determine the strain in the piezoresistive layer, the deflection of the beam is related to the curvature of a circle in Figure 6 where NPB is the neutral plane of segment A of the beam and NPP is the neutral plane of the piezoresistor. The distance from the neutral plane of the beam to the neutral plane of the piezoresistor is h . The derivation of the expression for strain is given in Appendix B resulting in:

$$\varepsilon = \frac{L_{NPP}(t) - L_{NPP}(0)}{L_{NPP}(0)} = \frac{h}{\alpha L^2} \frac{\partial y(\alpha, t)}{\partial u} \quad (3-15)$$

3.3. Instantaneous Resistance of Cantilever:

The vibration sensitivity relates the strain and resistance of the piezoresistive layer. The instantaneous value of the resistance of the piezoresistor is given by Geist(1997, 10):

$$R(t) = R(0)[1 + Z\varepsilon] \quad (3-16)$$

where Z is the piezoresistive coefficient defined as the ratio of the fractional change in the piezoresistor resistance to strain. By substituting the expression for strain found in Equation 3-15 into Equation 3-16, the instantaneous resistance of a cantilever becomes:

$$R(t) = R(0) \left[1 + \frac{Zh}{\alpha L^2} \frac{\partial y(\alpha, t)}{\partial u} \right] \quad (3-17)$$

Differentiating Equation 3-14 to obtain the slope of the beam and evaluating at $u=\alpha$ results in the expression:

$$\frac{\partial y(\alpha, t)}{\partial u} = \frac{y_o L^4 \omega^2 (3m_B [\alpha - \alpha^2] + m_A \alpha^3) \sin(\omega t)}{6(EI)_A} \quad (3-18)$$

By substituting Equation 3-18 into Equation 3-17, the instantaneous value of the resistance of the piezoresistive layer becomes:

$$R(t) = R(0) \left[1 + \frac{y_o Z L^2 \omega^2 h (3m_B [1 - \alpha] + m_A \alpha^2) \sin(\omega t)}{6(EI)_A} \right] \quad (3-19)$$

3.4. Piezoresistive Sensitivity:

Piezoresistive sensitivity relates the change in the resistance of an encapsulated piezoresistor to the amplitude, y_o , of a sinusoidal vibration driving the base of a cantilever. The piezoresistive sensitivity is different for each length cantilever and frequency. Another expression for instantaneous resistance is developed in Appendix C and by relating Equations 3-19 and C-9, the piezoresistive sensitivity of a single cantilever with an encapsulated piezoresistor becomes:

$$S_n = \frac{Z L_n^2 \omega^2 h (3m_B [1 - \alpha_n] + m_A \alpha_n^2)}{6(EI)_A} \quad (3-20)$$

3.5. Determination of the Piezoresistive Coefficient:

In order to determine the piezoresistive sensitivity, S , from Equation 3-20, the piezoresistive coefficient, Z , is needed. The coefficient is constant for all cantilevers in this study because all encapsulated piezoresistors used have the same properties and length. The piezoresistive coefficient is determined through a combination of theoretical and experimental means. A Wheatstone bridge is used to determine Z .

Wheatstone bridges are commonly used to determine unknown resistances. The development of an equation for a Wheatstone bridge with four different variable resistors is provided in Appendix D. The equation which relates the experimentally measured voltages to the piezoresistive sensitivity of each cantilever in the bridge is:

$$\Delta V_{\max} - \Delta V_{\min} = V_o y_o (S_2 + S_3 - S_1 - S_4) \quad (3-21)$$

When Equation 3-20 is substituted into Equation 3-21 for each cantilever sensitivity, the only unknown is the piezoresistive coefficient, Z. Having the value of Z allows for the calculation of S for any cantilever length and frequency.

4. Experimentation:

The instrumentation and equipment used in the experiments include a shaker table with frequency and amplitude controls, a MEMS package which includes a MEMS chip and external amplifier, an oscilloscope which displays voltage, and a voltage source which supplies a known voltage.

The experimentation included preliminary tests to determine if a signal could be seen from the piezoresistor in the cantilever when the chip was shaken with no amplification source. No signal was detected so a built-on amplifier was used with the cantilever, but the amplifier was found to be inoperable. An external amplifier was then chosen and used to try and attain a readable signal from the Wheatstone bridges (Bridge2, Bridge3, Bridge4) on the MEMS chip.

4.1. Preliminary Tests:

The first test performed on the MEMS was to determine if a voltage output could be attained from Bridge2. Bridge2 is located in the upper right corner of the chip seen in Figure 1. The chip was mounted in a 40-pin Cerdip (Ceramic Dual In Line Package) connector. The circuit diagram is set up as seen in Figure 3b. The chip and Cerdip connector were placed in the 40 pin chip holder that was mounted on the shaker table. A voltage source of ± 5 V was supplied to the Wheatstone bridge. The shaker table was set at a frequency of 60 Hz. The output of the Wheatstone bridge on the oscilloscope was a 8 mV peak to peak sinusoidal wave. As voltage increased, the signal remained constant. Therefore, this signal was created by noise.

A similar Wheatstone bridge (Bridge1) with the output connected to a built-on amplifier was then tested. This test determined if an output signal could be produced by the amplifier and tested the functionality of the amplifier. The circuit diagram for testing is found in Figure 7. The voltage, V_o (7), is 5 V supplied by a voltage source. The voltage (8) is put to ground. Position 5 is the positive voltage input to the amplifier from the Wheatstone Bridge, and 4 is the negative voltage input to the amplifier from the Wheatstone Bridge. The number 6 is the bias which must be tuned so that the output of 2 is zero. This gives zero offset voltage. In order to tune the output of 2 to zero the voltage

across 4 and 5 must equal zero. When this was done and the functionality of the amplifier was tested, it was found that the built-on amplifier did not operate because the output voltage remained approximately constant as the input voltage was changed, as seen in Figure 8. The next step in producing a visible signal from the Wheatstone bridge was to choose an external amplifier.

4.2. Selection of External Amplifier:

In order to choose an amplifier, the offset voltage of Bridge2 had to be determined. The offset voltage is the voltage difference between the two outputs of the Wheatstone bridge, $V_a - V_b$, in Figure 3b. In order to determine this offset voltage, the input voltage, $V_o - (-V_o)$, to the Wheatstone bridge was varied from 0.5 V to 1.5 V. The input voltages and the corresponding offset voltages are given in Table 1.

Table 1: Offset Voltage in Determining External Amplifier

Voltage In (V)	Offset Voltage (mV)
0.5	0.54
1	0.76
1.5	1.07

The amplifier was chosen to have an offset voltage less than the bridge offset voltage so that the signal from the amplifier could be read. The bridge offset voltage at a 1 V input was chosen to determine how low the amplifier offset voltage must be because all input voltages will be greater than 1V assuring that the amplifier will work.

An important characteristic of the external amplifier is that it has a low offset voltage so that small voltages from the MEMS test structure can be amplified. The external amplifier is in die form which means that the amplifier does not contain any external circuitry connections. A diagram of the Dice Characteristics is found in Figure 9 [Analog]. Because there are no external circuitry connections, the external amplifier die is packaged in the same Cerdip as the MEMS die and is wire bonded to it when the chips are wire bonded to the Cerdip pins.

4.3. Setup of Tests with MEMS and External Amplifier:

A diagram of the experimental set-up is shown in Figure 10. As seen in Figure 11, the MEMS package consists of a prototype MEMS (Figure 1) and an external amplifier (Figure 9). The shaker table is controlled with inputs of amplitude and frequency, and vertical motion is transmitted to the MEMS package. A known voltage of ± 5 V is supplied to one of the Wheatstone bridges on the MEMS and the external amplifier. The oscilloscope displays the voltage output from the MEMS package and the voltage created by the shaker table motion. The shaker table voltage can be equated to an acceleration of the MEMS package located on the shaker table piston with the use of a calibration table.

Two MEMS packages were tested. Each MEMS package contains half of a MEMS chip and two amplifiers. The package contains two amplifiers as a fail safe measure just in case one amplifier does not operate properly. Bridge3 is contained in Package1 and Bridge4 is contained in Package2. Packages 1 and 2 are seen in Figures 12 and 13, respectively. The packages were tested in the experimental set-up. The voltage supplied to Bridge3, Bridge4, and the amplifiers was ± 5 V. The frequency of the shaker table was set at 70 Hz so that any 60 Hz pick-up such as that which was observed earlier could be distinguished from the vibration signal.

4.3.1. Preparation Process of MEMS Package:

Epoxy is used as an adhesive to hold the chip and amplifier in place when connected to the Cerdip. A picture of a Cerdip is seen in Figure 11a. The package with the MEMS, amplifier, pin holder, and epoxy is placed in an oven preheated to 150°C . The oven heats up the resin so that it becomes solid and bonds the MEMS to the pin holder. The package is left in the oven for 30 minutes while the resin solidifies. After the chip is cooled, it is placed in an ultraviolet cleaner for five minutes, so the chip is cleaned before the etching process. For etching, the MEMS is placed inside a vacuum chamber at an etching station. When the MEMS is in place, the chamber is secured, and by the use of a computer, XeF_2 is pumped into the chamber. The gas reacts with bare silicon on the chip and removes it creating pits under the cantilevers. After the chip is etched, a wire bonding machine is used to bond a microscopic wire from one pin connection on the chip to another. A picture of the wire bonding machine is found in Figure 14.

5. Determination of Beam Properties:

The properties of the cantilevers are needed in order to determine the piezoresistive sensitivity. Properties needed are flexural rigidity and mass per unit length. The locations of the neutral planes of the cantilever and the piezoresistor in segment A must also be determined in order to calculate piezoresistive sensitivity.

5.1. Cantilever Model:

The beam characterizations are in the (x,y,z) coordinate system. The characteristics of the beam are seen below where the subscripts A and B represent the segment of the beam that is being described.

width:

$$w(x,y,z) = \begin{cases} w_A(y,z) & 0 \leq x \leq c \\ w_B(y,z) & c \leq x \leq L \end{cases} \quad (5-1)$$

mass density:

$$\rho(x,y,z) = \begin{cases} \rho_A(y,z) & 0 \leq x \leq c \\ \rho_B(y,z) & c \leq x \leq L \end{cases} \quad (5-2)$$

modulus of elasticity:

$$E(x,y,z) = \begin{cases} E_A(y,z) & 0 \leq x \leq c \\ E_B(y,z) & c \leq x \leq L \end{cases} \quad (5-3)$$

mass per unit length:

$$m(x) = \begin{cases} m_A = \int_0^{h_A} \int_0^{w_A(y)} \rho_A(y,z) dz dy & 0 \leq x \leq c \\ m_B = \int_0^{h_B} \int_0^{w_B(y)} \rho_B(y,z) dz dy & c \leq x \leq L \end{cases} \quad (5-4)$$

flexural rigidity (equivalent stiffness):

$$EI(x) = \begin{cases} EI_A = \int_0^{h_A} \int_0^{w_A(y)} E_A(y, z) y^2 dz dy & 0 \leq x \leq c \\ EI_B = \int_0^{h_B} \int_0^{w_B(y)} E_B(y, z) y^2 dz dy & c \leq x \leq L \end{cases} \quad (5-5)$$

In order to describe beam properties, the properties of the materials that make up the beam must be known. Table 2 gives the properties of the materials. Figure 5 shows the location of the materials in segment A. Segment B contains only one material, silicon oxide.

Table 2: Properties of Materials [Brand, 1994]

Material	E (GPa)	ν (Poisson's Ratio)	ρ (kg/m ³)
Polysilicon	150	0.17	2300
Silicon Oxide	70	0.17	2200

A physical layer is a plane of material in the x-z plane. If a different material is encountered in the x-z plane as y increases from y=0 to y=H then there is a new physical layer. Figure 15 shows the physical layers of segment A and segment B. The dimensions of the materials in segment A and segment B are found in Figure 5.

5.2. Determination of Flexural Rigidity and Mass per Unit Length:

The beam dimensions, flexural rigidity, and the mass per unit length are used to determine the properties for each physical layer by assuming that the materials are isotropic. Once the properties of the physical layers are calculated, the values for flexural rigidity and mass per unit length can be determined for each segment of the beam by adding the properties of the physical layers in the segment. The calculations were done using Equations 5-4 and 5-5 and are found in Appendix E. The properties of each segment of the beam are provided in Table 3.

Table 3: Beam Properties

Segment	EI (Flexural Rigidity) (kg/ms ²)	m (kg/m)
A	$3.71 \cdot 10^{-11}$	$2.169 \cdot 10^{-7}$
B	$3.701 \cdot 10^{-11}$	$2.167 \cdot 10^{-7}$

5.2.1. Location of Neutral Planes:

The determination of the distance between the neutral planes of the piezoresistor and segment A of the beam is necessary to determine the strain in the piezoresistor and the piezoresistive sensitivity. The neutral plane of the piezoresistors is the x-z plane that bisects the piezoresistors. The neutral plane of the beam for segment A is found through the use of the moment of areas about a chosen axis on the beam and solving for the neutral axis. Because segment A is made of different materials, the areas of the different materials are related with the use of elasticity properties. The calculations for determining the neutral plane of segment A are found in Appendix F. Figure 6 illustrates the location of the neutral planes. Table 4 gives the y location of the neutral planes and the distance h between the planes.

Table 4: Neutral Plane Locations in Relation to y=0 and Separation Distance

Piezoresistor's Neutral Plane (μm)	0.8
Segment A's Neutral Plane (μm)	1.9522
h (μm)	1.1522

6. Results/Discussion:

The circuit structures on the chip were initially tested to determine their operability. These circuit structures included two Wheatstone bridge setups (Bridge1 and Bridge2) and an amplifier which is connected to Bridge1. It was found that no output voltage could be read from Bridge2 by itself and that Bridge1's built-on amplifier did not work. A suitable external amplifier was then chosen that could operate with each of the Wheatstone bridges being tested. The piezoresistive sensitivity was then determined for each of the cantilevers lengths. The sensitivity was determined through the use of theory and experimentation.

6.1. Gain of the External Amplifier:

The gain of the external amplifier is of particular importance in relating the theory and experimentation. Tests were performed to determine the gain of the amplifier. When the amplifier was in the test Package2 and tested with no motion, the gain was determined to be 57.8. The gain data, amplifier output voltage versus amplifier input voltage is found in Figure 16. The gain is the slope of the line. Package1 gain was determined in similar fashion and found to be 42.8.

6.2. Piezoresistive Sensitivity:

Three tests were performed to determine the piezoresistive coefficient, Z . Once the piezoresistive coefficient is determined, the piezoresistive sensitivity can be calculated for any length cantilever of the type used in this study. An example of an oscilloscope reading for Package2 at 70 Hz is seen in Figure 17. In the figure, the top sinusoidal voltage is the output from the shaker table and the bottom voltage reading is the output from the MEMS package. The peak-to-peak voltage from the MEMS package gives $\Delta V_{\max} - \Delta V_{\min}$ used in Equation 3-21. The peak-to-peak voltage and frequency of the shaker table are used with a Table 5 [NIST, 1998] to determine the acceleration.

Table 5: Frequency Relation to Sensitivity used to Determine Acceleration in Volts

Frequency (Hz)	Sensitivity (mV/g)
50	20.44
100	20.36

Using Equations 3-20 and 3-21 together allows for the calculation of Z . The value for Z ranges from 130 to 260, and its value for use in future tests is 190. A sample calculation for determining Z is found in Appendix G, and the results from the experiments are seen below in Table 6.

Table 6: Results from Testing of Packages

Package	1	2	2
Frequency (Hz)	70	70	90
Acceleration (m/s^2)	144	144	173
$\Delta V_{\text{max}} - \Delta V_{\text{min}}$ from Package (V)	0.015	0.023	0.027
$\Delta V_{\text{max}} - \Delta V_{\text{min}}$ from Shaker Table (V)	0.3	0.3	0.35
Gain	42.8	57.8	57.8
Z	130-260	190	190

The variation in Z is due to variation in cantilever design. One of the 0.8 mm cantilevers in Bridge3 is supported by metal at its base which does not allow as much deflection as the other 0.8 mm cantilever in the Wheatstone bridge. Two calculations were performed to get a range for Z because of the difference in cantilevers. The first calculation assumes that both cantilevers deflect the same amount giving them the same instantaneous resistance. The value of Z calculated by this method is the lower value of Z found in Table 5 for Package1. The second calculation assumes that the 0.8 mm cantilever supported by the metal is rigid. By using this assumption, the Wheatstone bridge would appear to have one 0.8 mm cantilever and three reference cantilevers. The value of Z calculated by this method was 260. This means that the piezoresistive coefficient is $130 < Z < 260$. The

average value of Z calculated from Package2 which is shown in Table 6, 190, falls into this range and is the piezoresistive coefficient that was determined for the polysilicon piezoresistor. The piezoresistive coefficient from Package2 is used to determine the piezoresistive sensitivities as a function of length for frequencies from 20 Hz to 90 Hz in Figure 18. A sample calculation of the piezoresistive sensitivity is found in Appendix H.

6.3. Best Design Length of Cantilever:

The shortest acceptable cantilever length is controlled by the lowest frequency and acceleration of the compressor to be monitored. In order to determine the acceptable cantilever length, the acceleration must be known at 20 Hz. In all experiments the amplitude remained constant, so with a known frequency the maximum acceleration could be calculated for any frequency. At 20 Hz, the calculated acceleration is 11.8 m/s^2 . With this acceleration and an external amplifier, the shortest acceptable length among the cantilevers tested is 1.6 mm.

Figure 18 and Equation 3-20 show that, as the cantilever length and frequency increase, the piezoresistive sensitivity increases. The piezoresistive sensitivity increases approximately quadratically with the length of the cantilever because length appears in Equation 3-20 both as L^2 and in α , the ratio of the piezoresistor length to the beam length. Thus, the most sensitive cantilever design is the longest cantilever. As the length of the cantilever increases, however, problems occur.

The main problem is the breaking of the cantilever which can occur in the etching process or even during post-etch handling of the chip. Etching is not uniform due to the way that the XeF_2 reacts with the silicon, causing residual stresses in the cantilever that can lead to breakage of the longer cantilevers.

Another concern with longer cantilevers is having the cantilever touch the bottom of the chip with its vertical motion. Figure 19 shows the deflection of varying length cantilevers at varying frequencies of the shaker table for an acceleration of 144 m/s^2 determined from Equation 3-16 of the theory section. Cantilevers at 90 Hz could be up to 2.9 mm in length before they hit the bottom of the etched pit at 90 Hz which is $0.125 \text{ }\mu\text{m}$ deep.

If the etching process, post handling, and packaging of the MEMS chip could be refined so as not to break any cantilevers, the cantilever design length can be a maximum length of 2.9 mm. Because the etching process using XeF_2 is difficult to refine, the best length cantilever should be a length of 1.6 mm. If an on-chip amplifier is used and noise is reduced, signals from cantilever with lengths less than 1.6 mm may be detectable even at the lowest frequencies. As such, the acceptable cantilever length could be less than 1.6 mm.

6.4. Effects of Noise on Experimentation:

Because the amplifier and Wheatstone bridges were not integrated on a single chip, external wires were necessary in the experimental set-up. As a result, noise was a factor. All wires in the experimental set-up acted as antennas due to their open loops and created noise. Figure 20 shows a noise pick-up of 0.8 mV when the shaker table was off. Figure 21a is the reading on the oscilloscope for the experimental set-up seen in Figure 21b for the testing of package2. The wires in Figure 21b are open loops that create electrical fields and extra noise while testing. Figure 21c is the reading on the oscilloscope for the experimental set-up seen in Figure 21d. The wires in this set-up have been twisted together reducing the electrical field and giving a signal with less noise than the 8mV.

Experiments were done on Package1 and Package2. The experimental voltages from the amplifier for various length cantilevers are found in Figure 22. Noise of 8 mV is combined with both sinusoidal signals. A theoretical calculation of what the voltage would be for a Wheatstone bridge containing two 0.4 and two reference cantilevers was determined and is shown in Figure 22 also. Thus, the 0.4 cantilever was determined to be not sensitive enough to create a voltage greater than the noise. The 0.4 mm cantilever and noise voltages were approximately the same which means that longer length cantilevers are needed in the bridge to get a readable signal with this experimental set-up, having an off-chip amplifier.

7. Conclusions and Recommendations:

Trough this research a method was developed that relates beam theory to MEMS testing, allowing the determination of the sensitivity for any cantilever geometry for any future designs. In the present study, the piezoresistive sensitivities were calculated to determine the piezoresistive coefficient, $Z=190$. Piezoresistive sensitivity increased with length of the cantilever and the frequency of the shaker table.

The built-on amplifier connected to Bridge1 did not work. An external amplifier was chosen and Package1 and Package2 were tested to determine which cantilevers could produce signals with an external amplification. The 0.4 mm cantilever with an external amplifier was not sensitive enough to produce a voltage greater than the voltage created by noise, but the 0.8 mm and 1.6 mm cantilevers were sensitive enough at 70 to 90 Hz.

The maximum length cantilever was theoretically determined to be 2.9 mm for a frequency operating range of 20-90 Hz. A cantilever length of greater than 1.6 mm is not recommended due to the problems of breakage that occur in the etching process and post-etch handling. Because the cantilevers must detect vibrations at frequencies as low as 20 Hz, the 0.8 mm cantilever is not sensitive enough if an off-chip amplifier is used. The best length cantilever if an external amplifier must be used is 1.6 mm.

Future testing with a built-on amplifier is recommended to reduce noise and cost. A reduction in noise may make other cantilever lengths sensitive enough at the desired frequencies. Cost reduction, critical to commercialization, is possible if the amplifier is on the chip. The residual stresses resulting from etching point to the need for durability testing of the chip in a variety of orientations.

References

- Baltes, Henry. "CMOS as Sensor Technology." Sensors and Actuators. A, Physical, 37-38, 1993, 51-56.
- Brand, Oliver. "Micromachined Resonators for Ultrasound based Proximity Sensing." Physical Electronics Laboratory, Zurich. Diss. Eth. No. 10896, 1994.
- Chiriac, H., Urse, M., Rusu, F., Hison, C., Neagu, M. "Ni-Ag Thin films as Strain-Sensitive Materials for Piezoresistive Sensors." Sensors and Actuators. A, Physical, 76, 1999, 376-380.
- Didion, David. "Thinking Really Small." HVAC and R Research, 4, 1, Jan 1998.
- Geist, Jon. "Task 4 Final Report," July 7, 1998.
- Geist, Jon. "Final Report for NIST Order Number 43NANB713075: Development of an analytical model for the sensitivity of a cantilever-type, piezoresistive, CMOS-Integrated Circuit Foundry (CIF) MicroelectroMechanical Systems vibration sensor," October 14, 1997.
- Geist, Jon. Personal Conversation, Fall Semester, 1999.
- NIST. Calibration Table for Shaker Table, accelerometer manufacturer: Endevco, model: 2270M1, sn:B19; signal conditioner: Bruel and Kjaer, model: 2626, sn 729260, 1998.
- Paula, Greg. "MEMS Sensors Branch Out." Mechanical Engineering, Oct. 1996, 64-68.
- Petersen, K., Shartel, A., Raley, N. "Micromechanical accelerometer integrated with MOS detection circuitry," IEEE Trans. Electron Devices, ED-29, Jan. 1982.
- Riley, W.F., Zachary, L. Introduction to Mechanics of Materials. John Wiley and Sons, New York, 1989.
- Stemme, Goran. "Resonant Silicon Sensors." Journal of Micromechanical Microengineering, 1, 1991, 113-125.
- Su, Y., Brunnschweiler, A., Evans, A.G., Ensell, G. "Piezoresistive Silicon V-AFM Cantilevers for High-Speed Imaging." Sensors and Actuators. A, Physical, 76, 1999, 139-144.
- Thomson, W.T. Theory of Vibration with Applications. Prentice Hall, Englewood Cliffs, New Jersey, 1998.

Van Mullem, C.J., Blom, F.R., Fluitman, H.J., Elwenspoek, M. "Piezoelectrically Driven Silicon Beam Force Sensor." Sensors and Actuators. A, Physical, 25-27, 1991, 379-383.

Web site: http://analog.com/pdf/preview/AMP01_c.gif

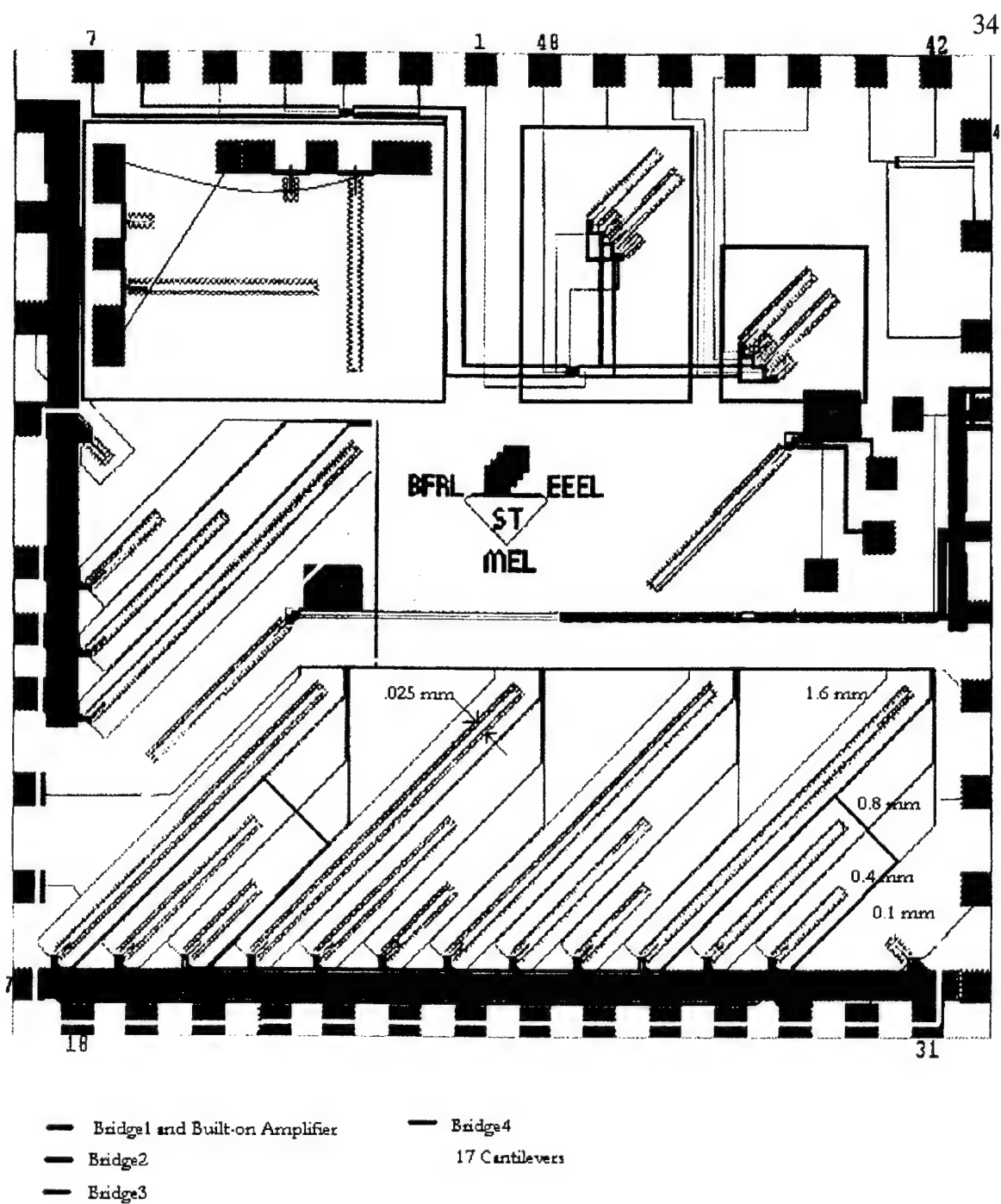
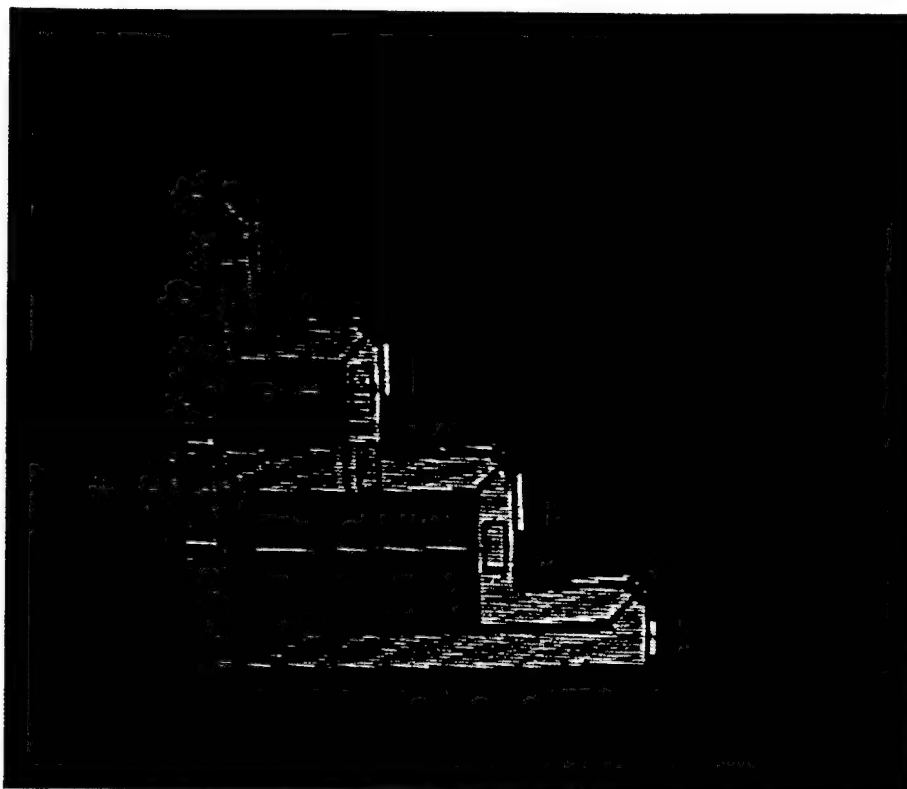
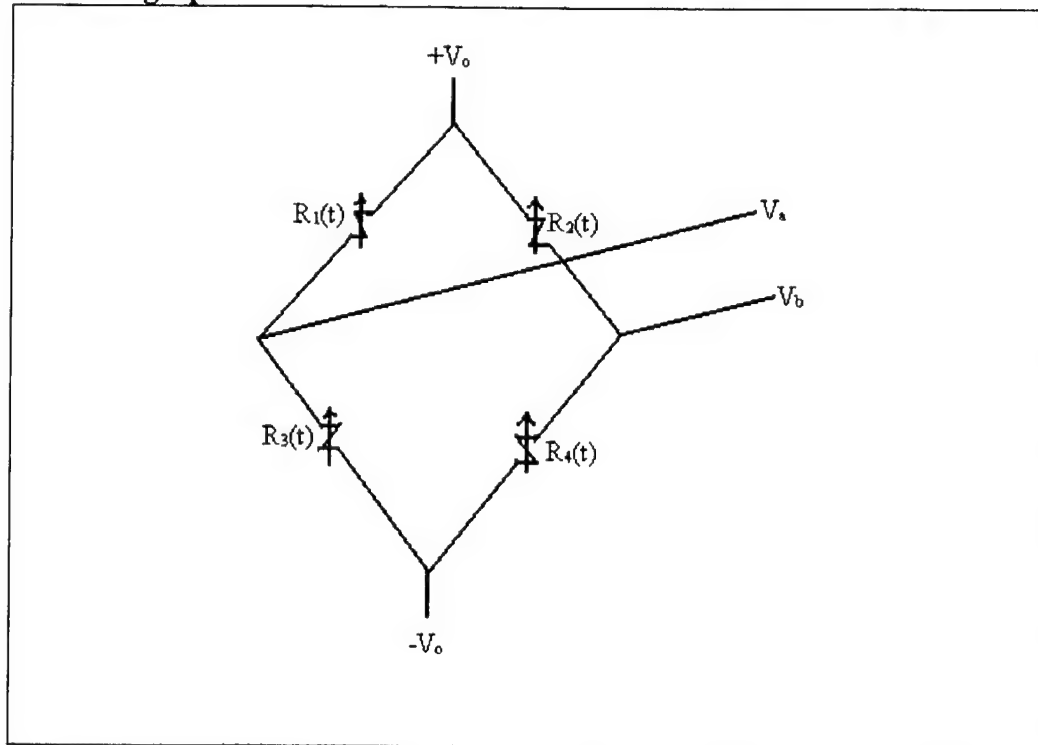


Figure 1: Schematic of Prototype MEMS



Figure 2: Close Up View of A Typical Cantilever

**3a: Photograph****3b: Circuitry Diagram****Figure 3: Wheatstone Bridge Details**

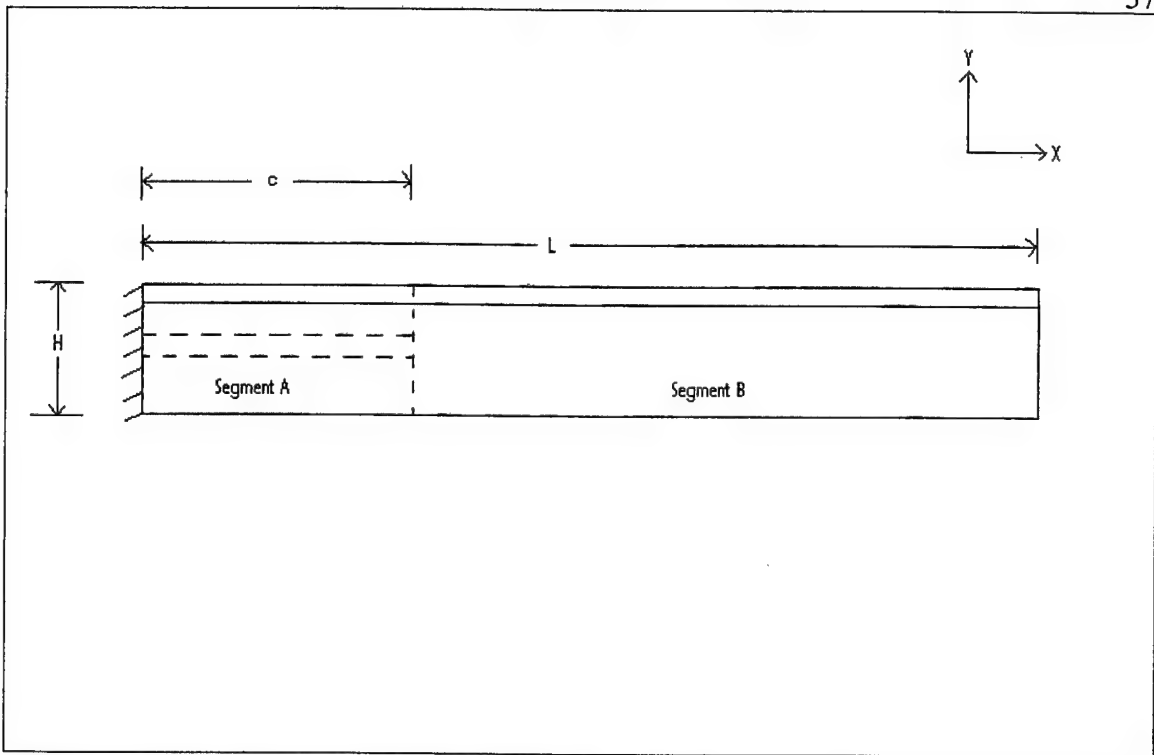


Figure 4: Side-view of a Typical Cantilever

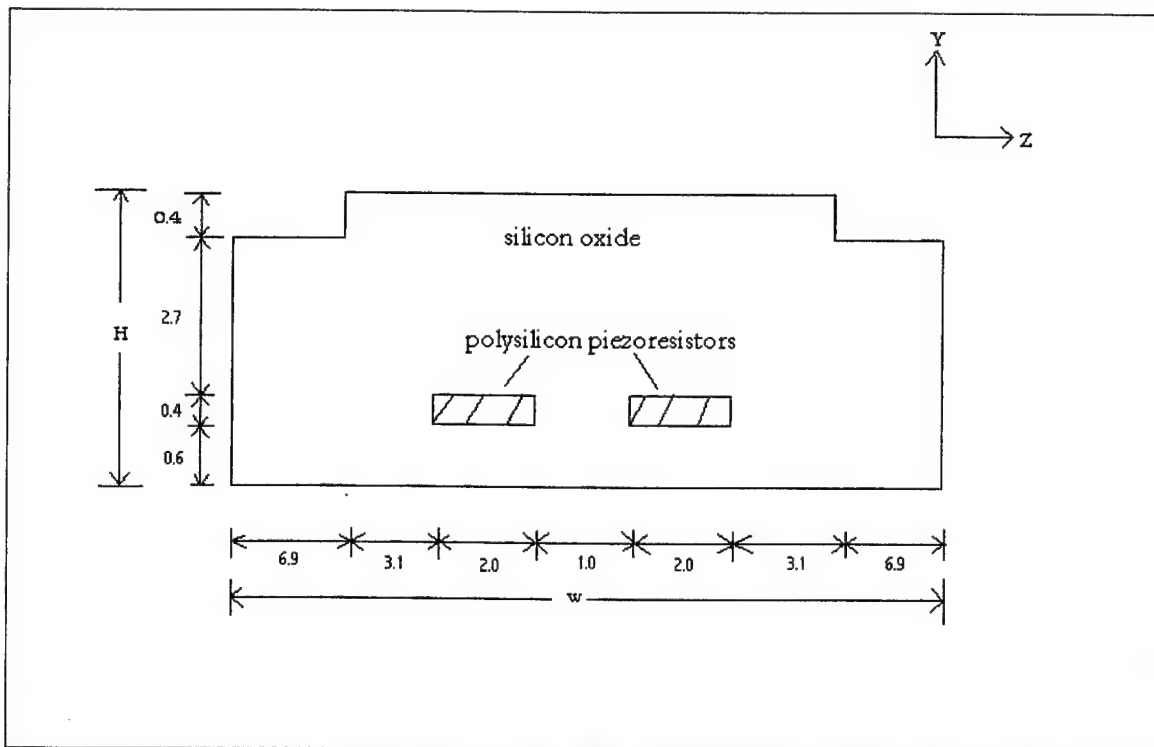


Figure 5: Cross Section of Segment A of a Typical Cantilever (Length in μm)

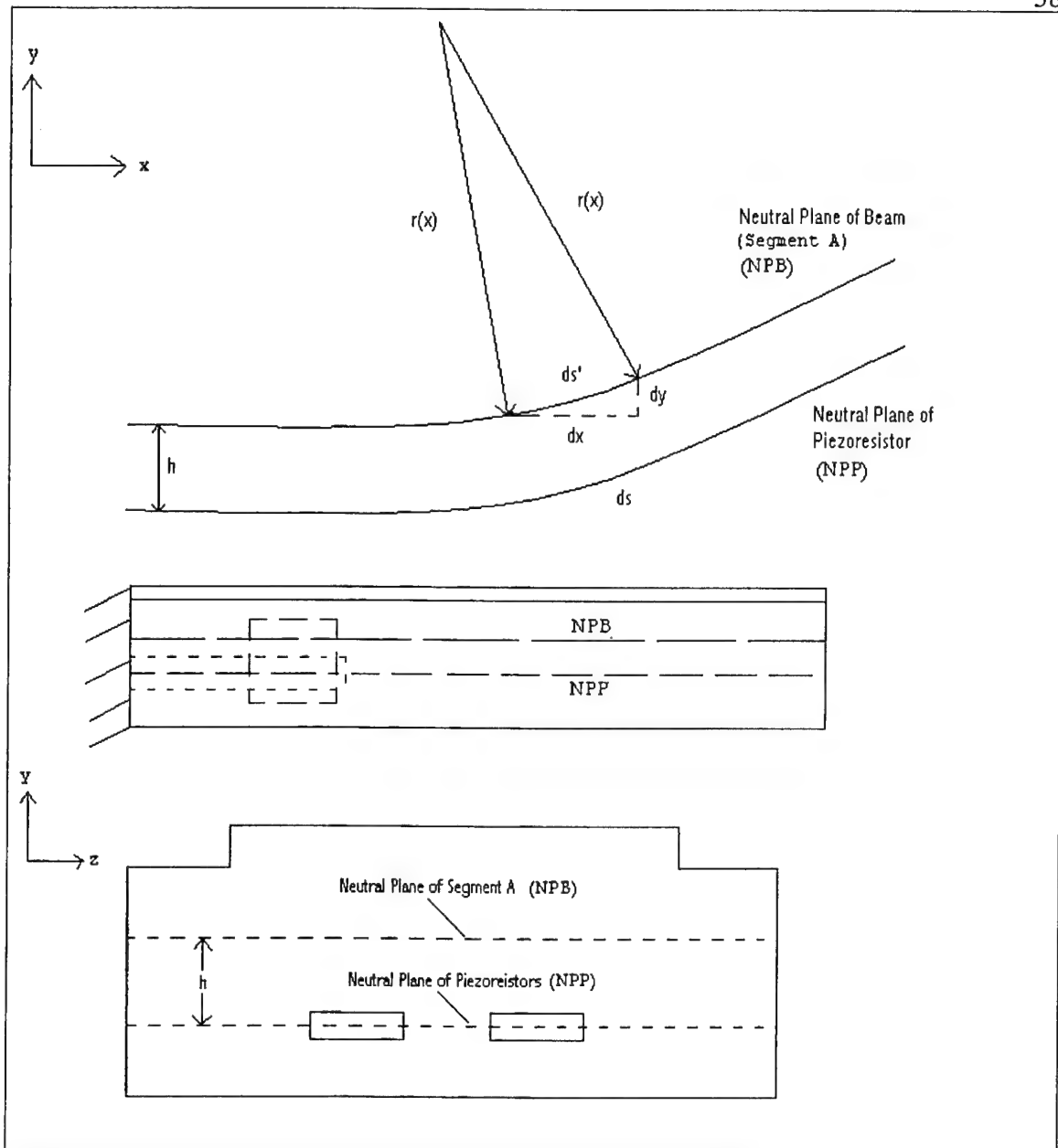


Figure 6: Local Radius of Curvature of a Typical Cantilever

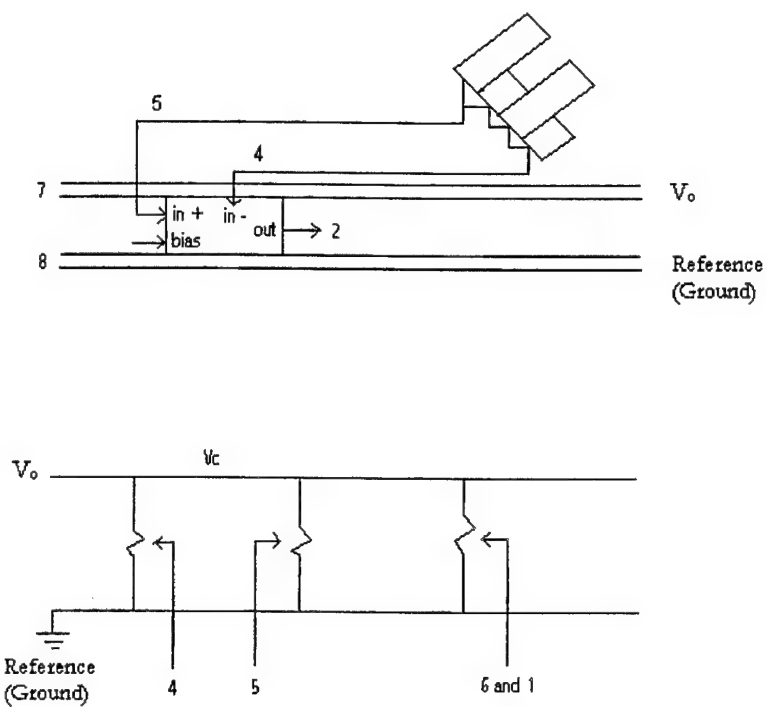


Figure 7: Circuitry to Test Operability of Built-on Amplifier for BRIDGE1

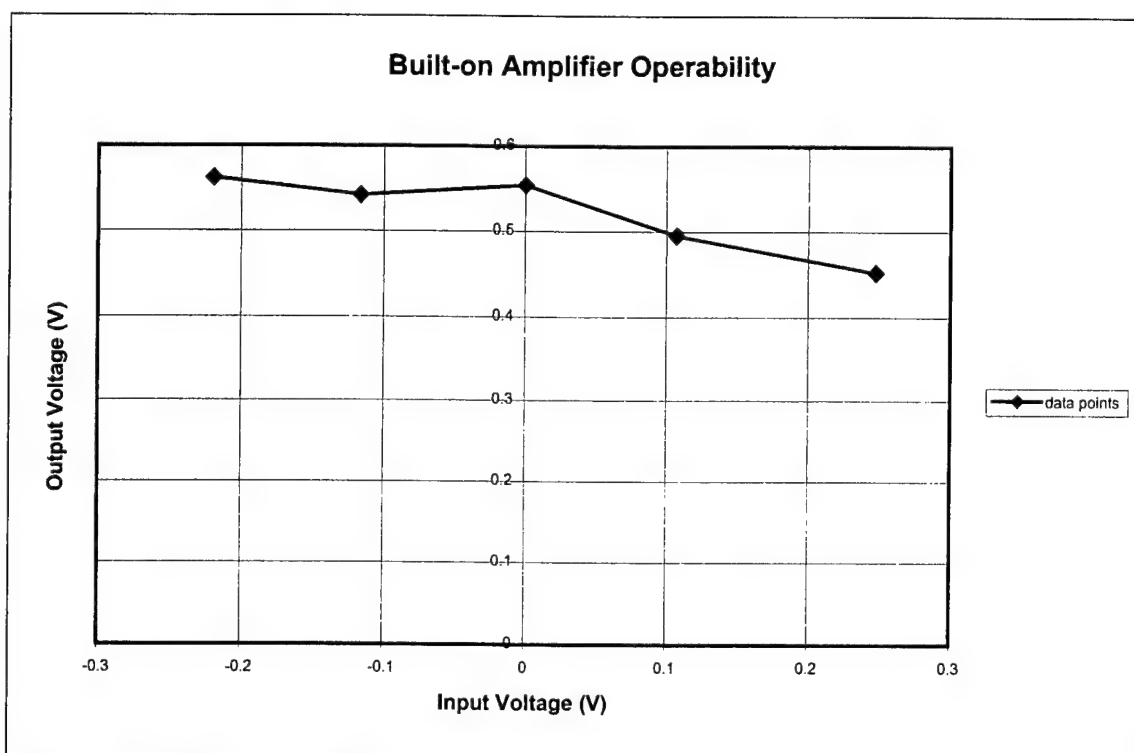
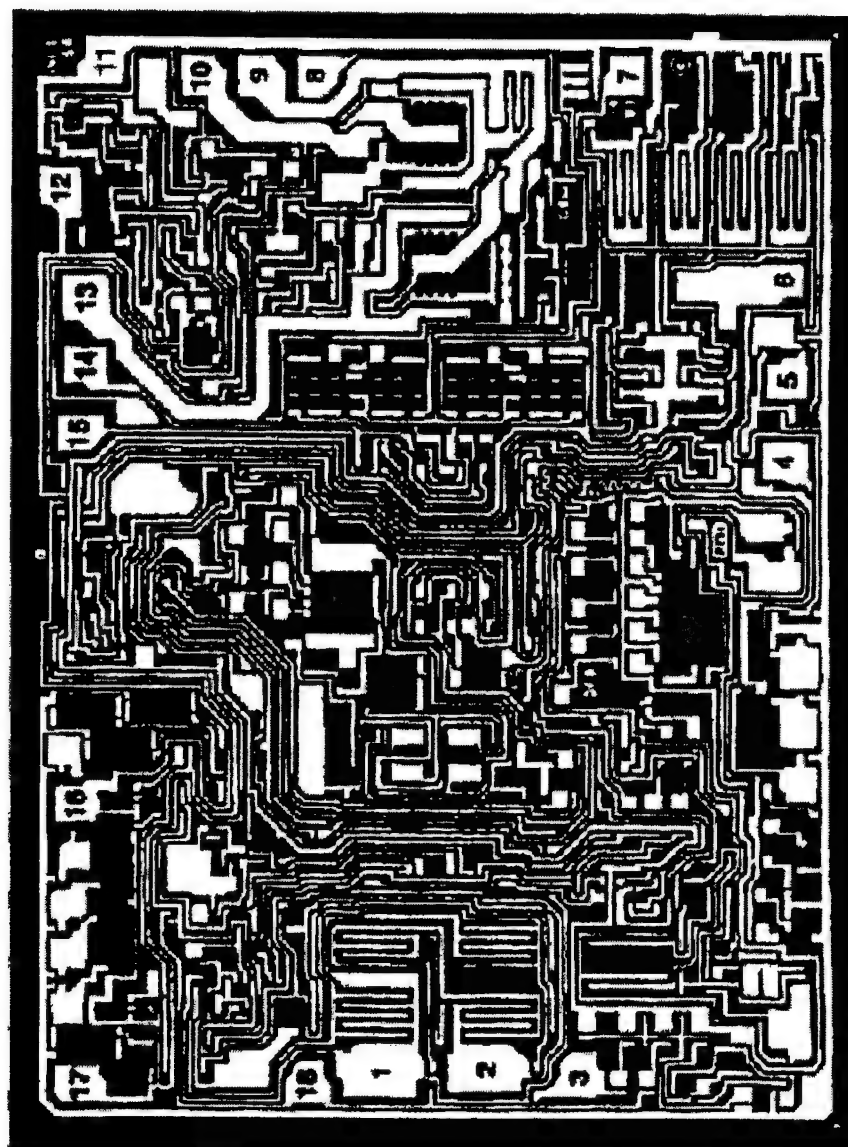


Figure 8: Built on Amplifier Data

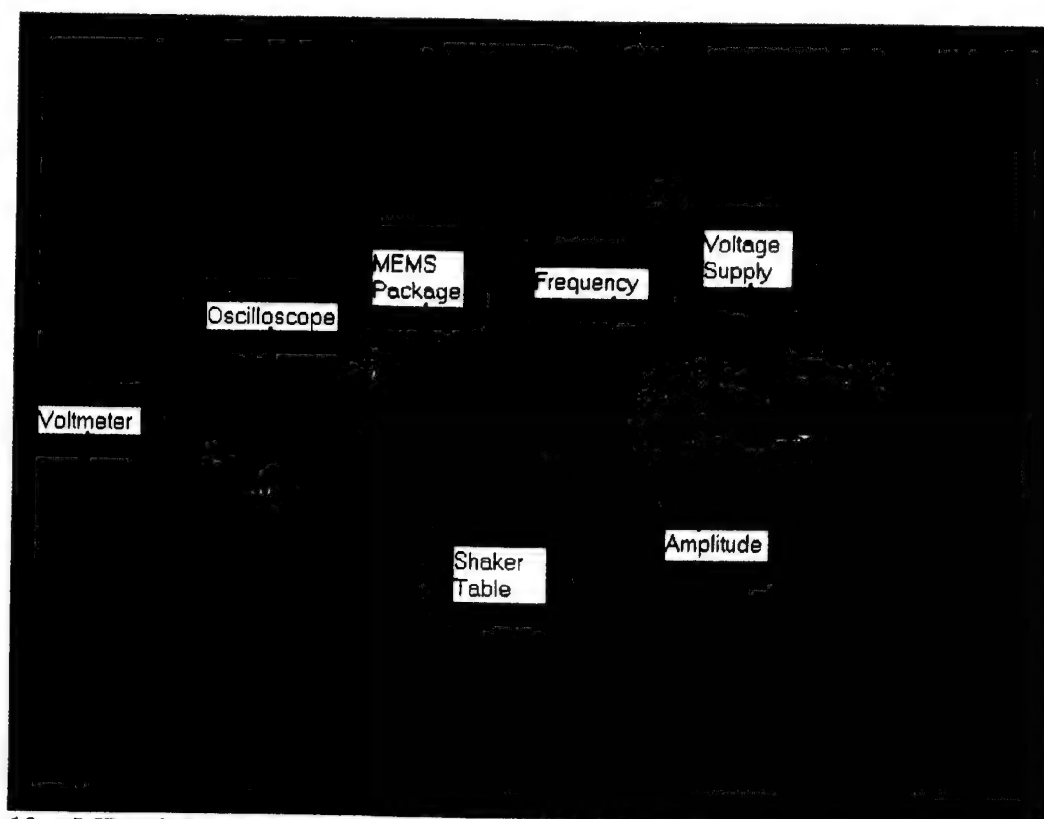
DICE CHARACTERISTICS

Die Size 0.111 x 0.149 inch, 16,539 sq. mils
(2.82 x 3.78 mm, 10.67 sq. mm)

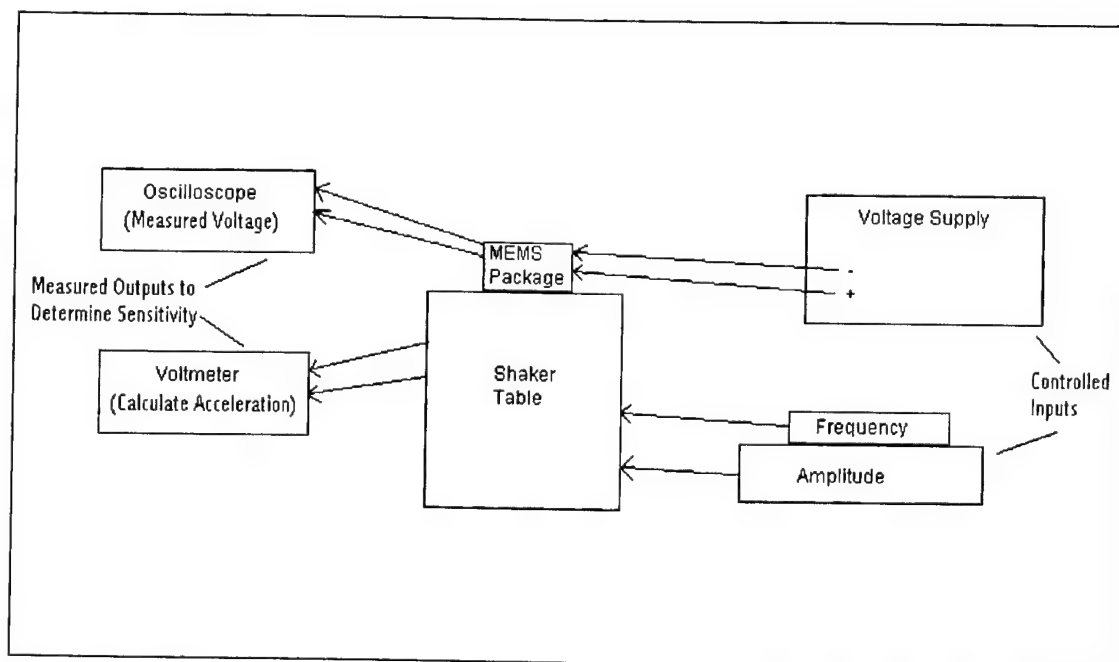


- | | |
|------------------|--------------------|
| 1. R_0 | 10. V_- (OUTPUT) |
| 2. R_0 | 11. V_- |
| 3. -INPUT | 12. V_+ |
| 4. V_{OS} NULL | 13. V_+ (OUTPUT) |
| 5. V_{OS} NULL | 14. R_3 |
| 6. TEST PIN* | 15. R_3 |
| 7. SENSE | 16. V_{OS} NULL |
| 8. REFERENCE | 17. V_{OS} NULL |
| 9. OUTPUT | 18. -INPUT |
- * MAKE NO ELECTRICAL CONNECTION

Figure 9: External Amplifier (AMP01 NBC) Characteristics

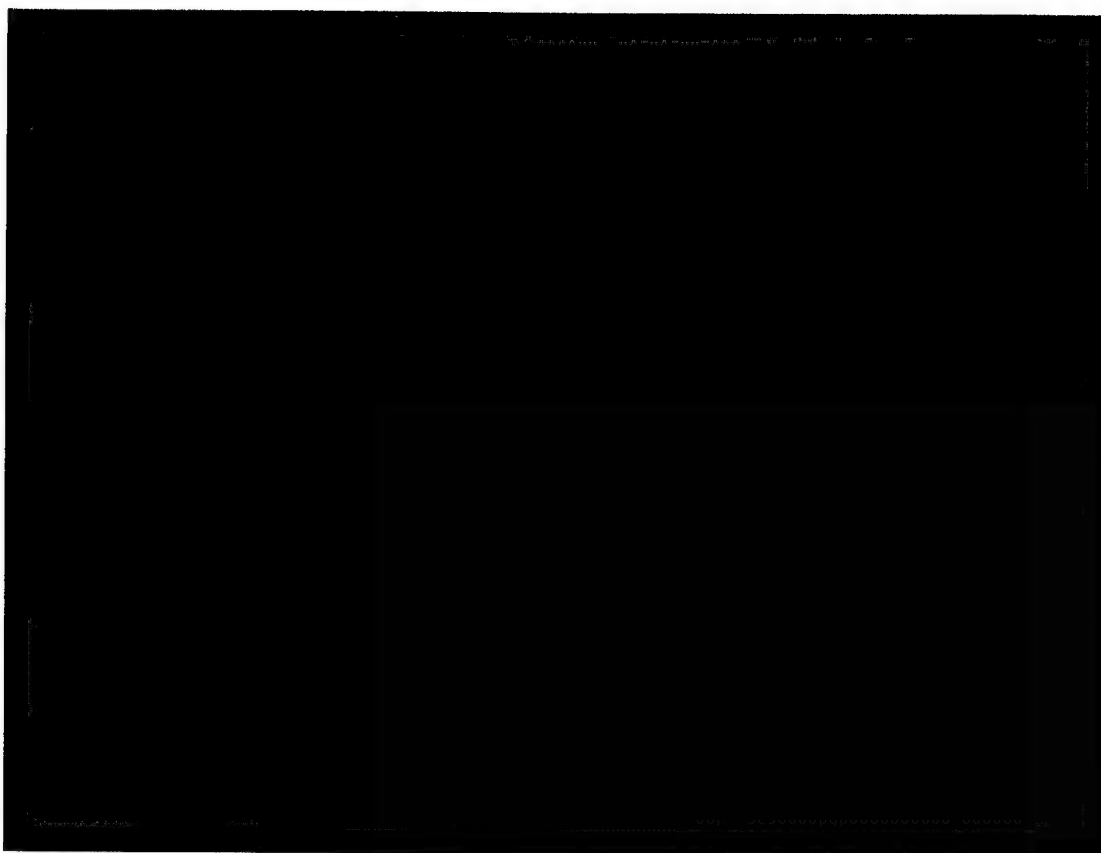


10a: MEMS Lab Photograph

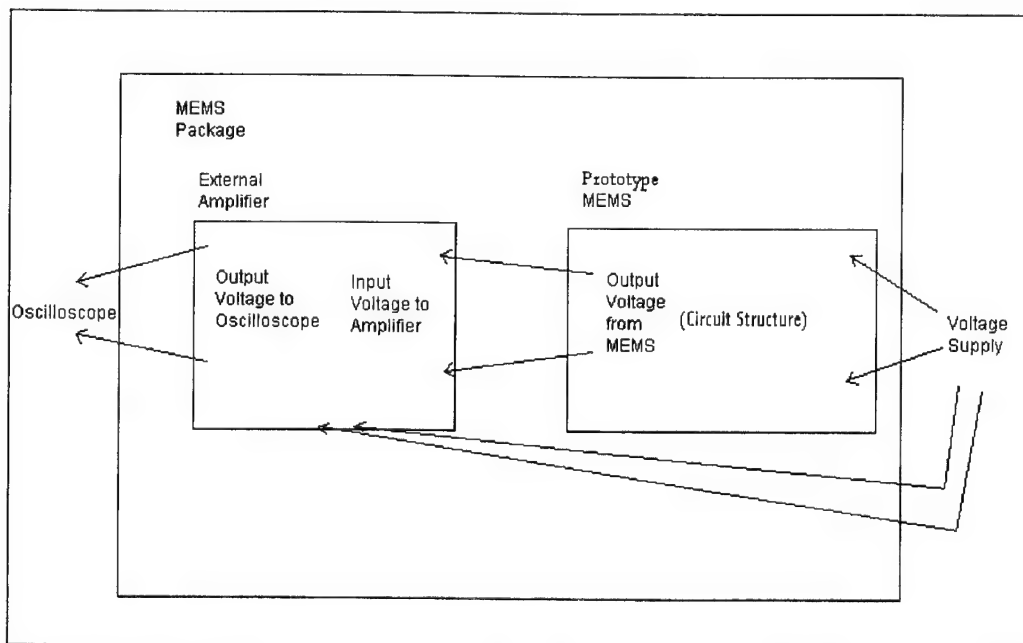


10b: Line Diagram

Figure 10: MEMS Testing Equipment Set-up



11a: Photograph



11b: Line Diagram

Figure 11: Typical MEMS Package in a Cerdip Die Well

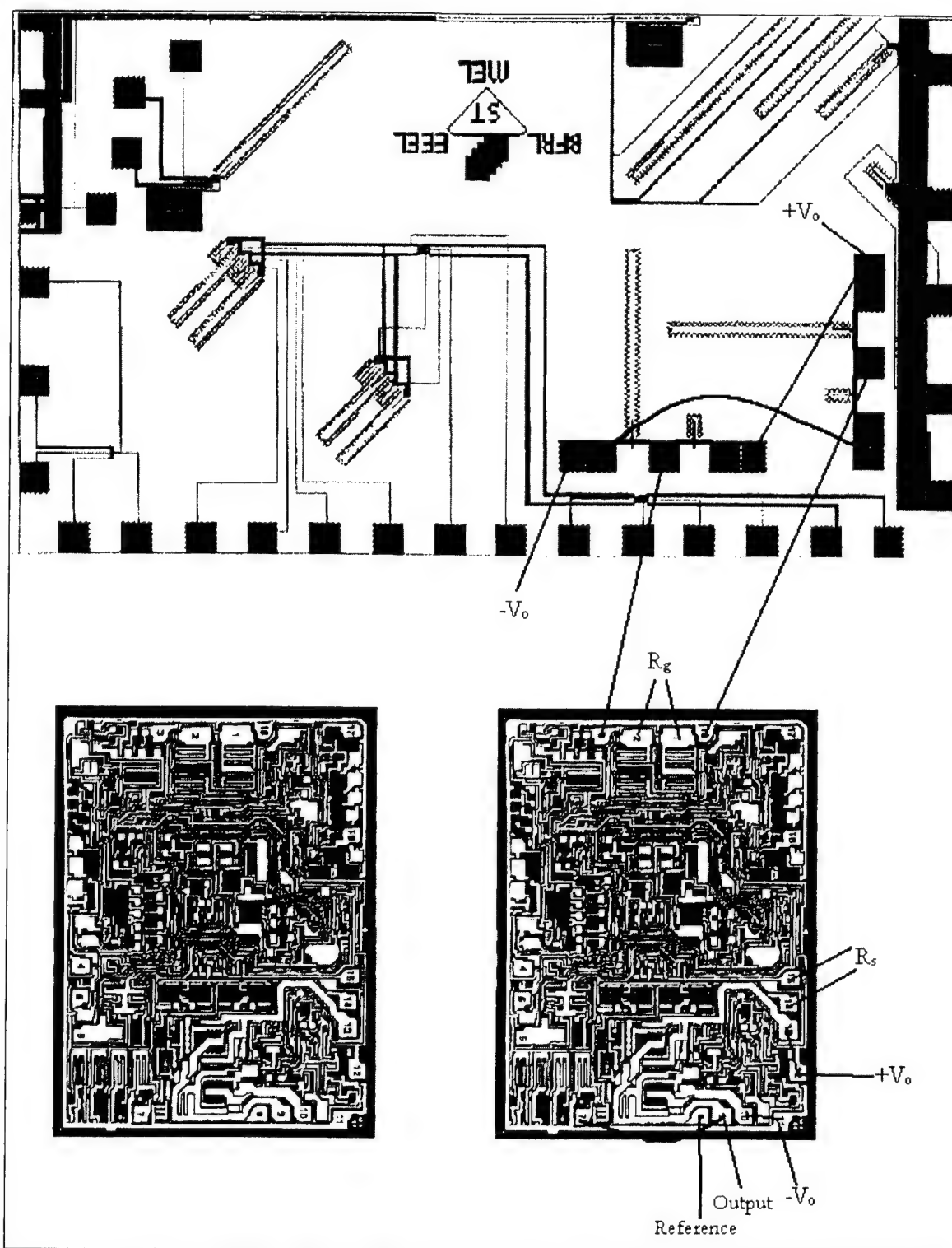


Figure 12: Package1 (Bridge3 with External Amplifier)

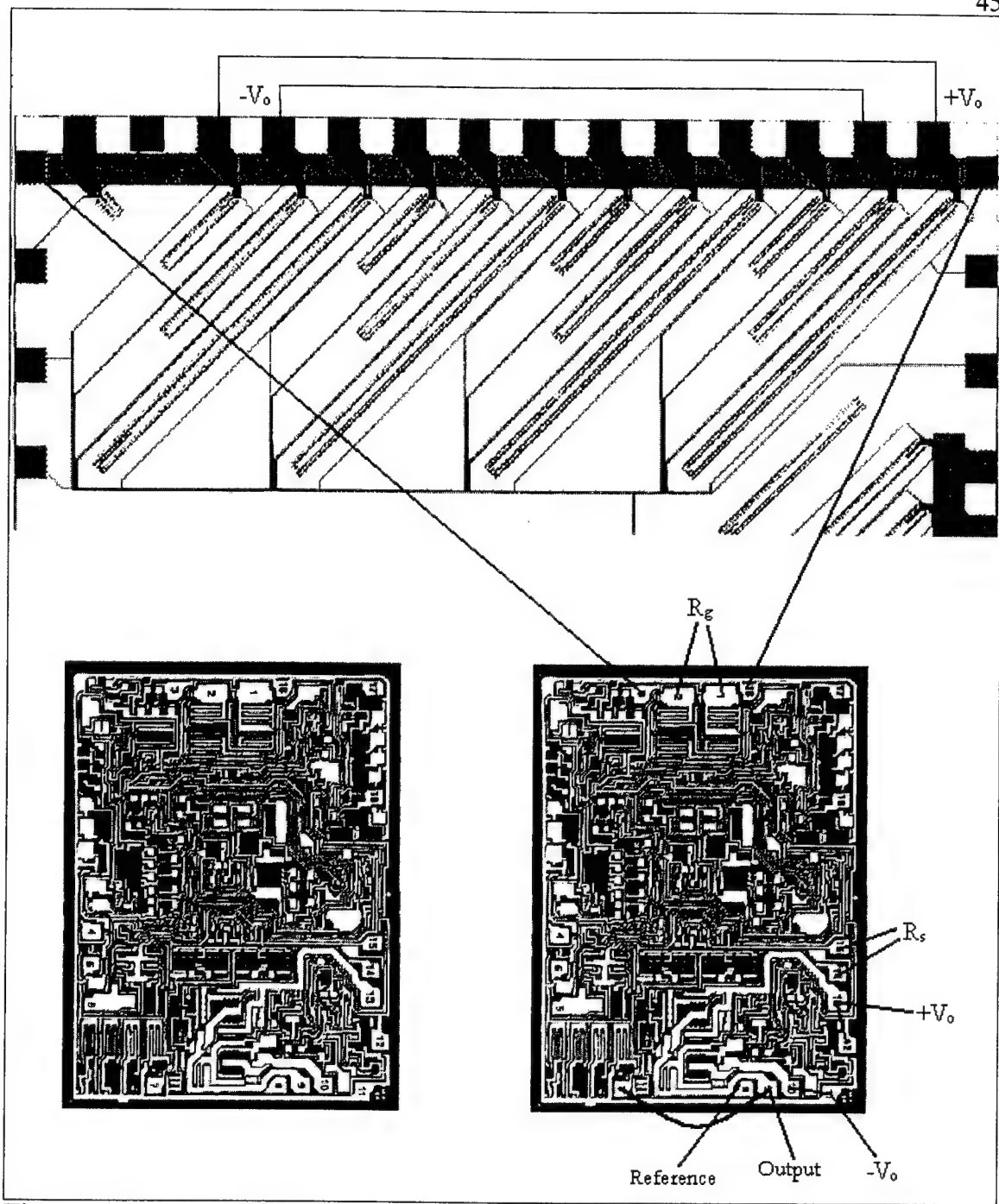


Figure 13: Package2 (Bridge4 with an External Amplifier)

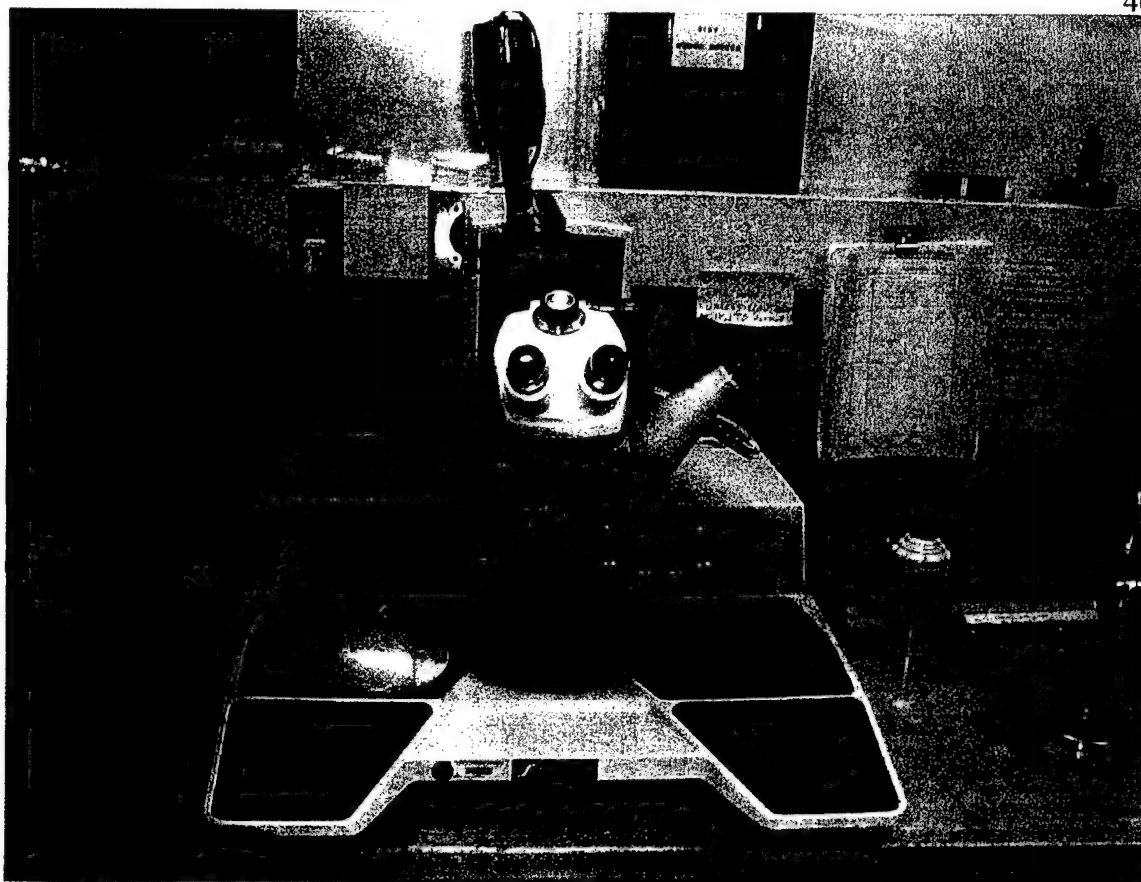
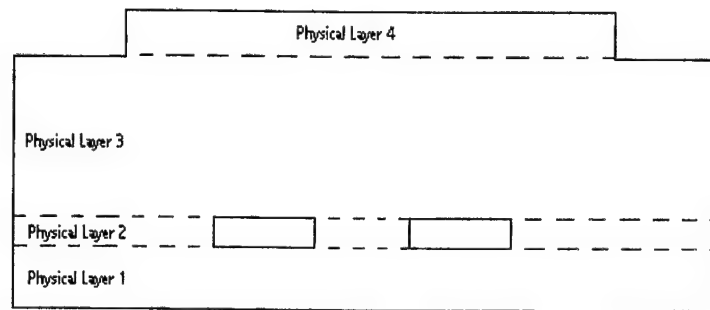
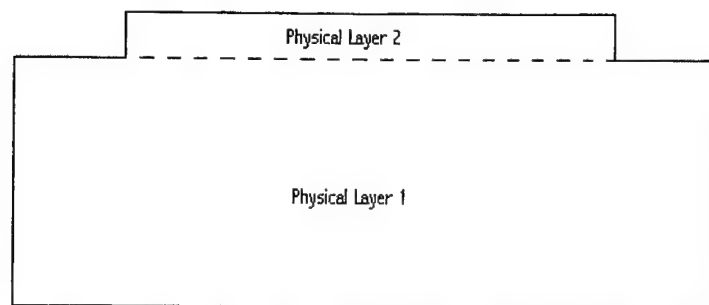


Figure 14: Wire Bonding Machine



Physical Layers of Segment A



Physical Layers of Segment B

Figure 15: Physical Layers of Beam

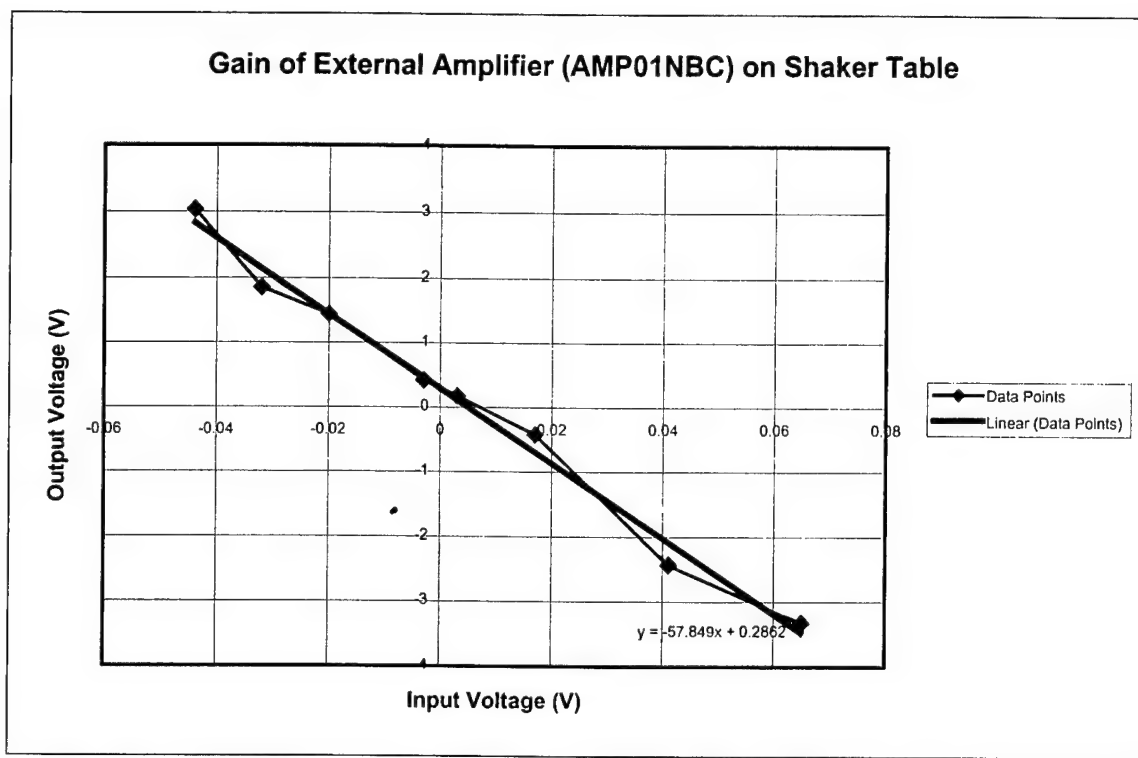


Figure 16: Gain of External Amplifier (AMP01 NBC) on Shaker Table

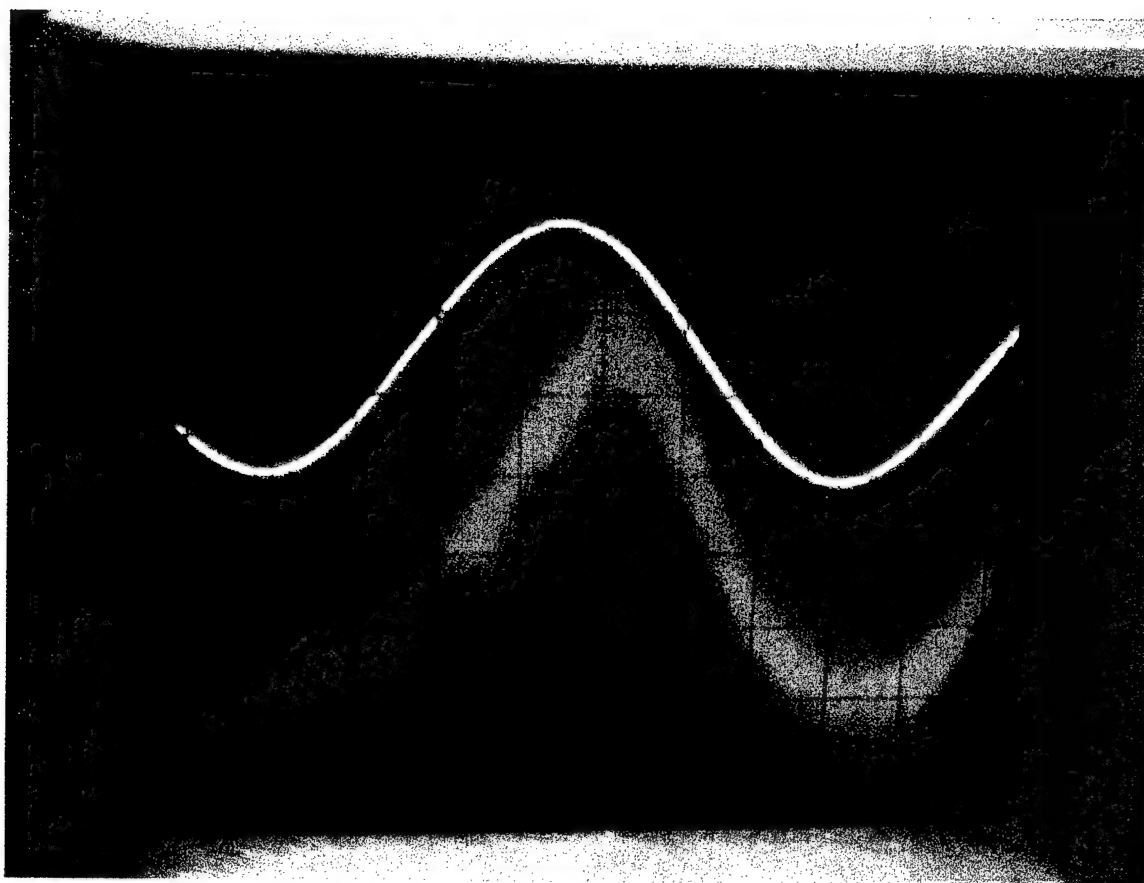


Figure 17: Oscilloscope Reading (Upper Voltage – Shaker Table; Lower Voltage – Output from Package2)

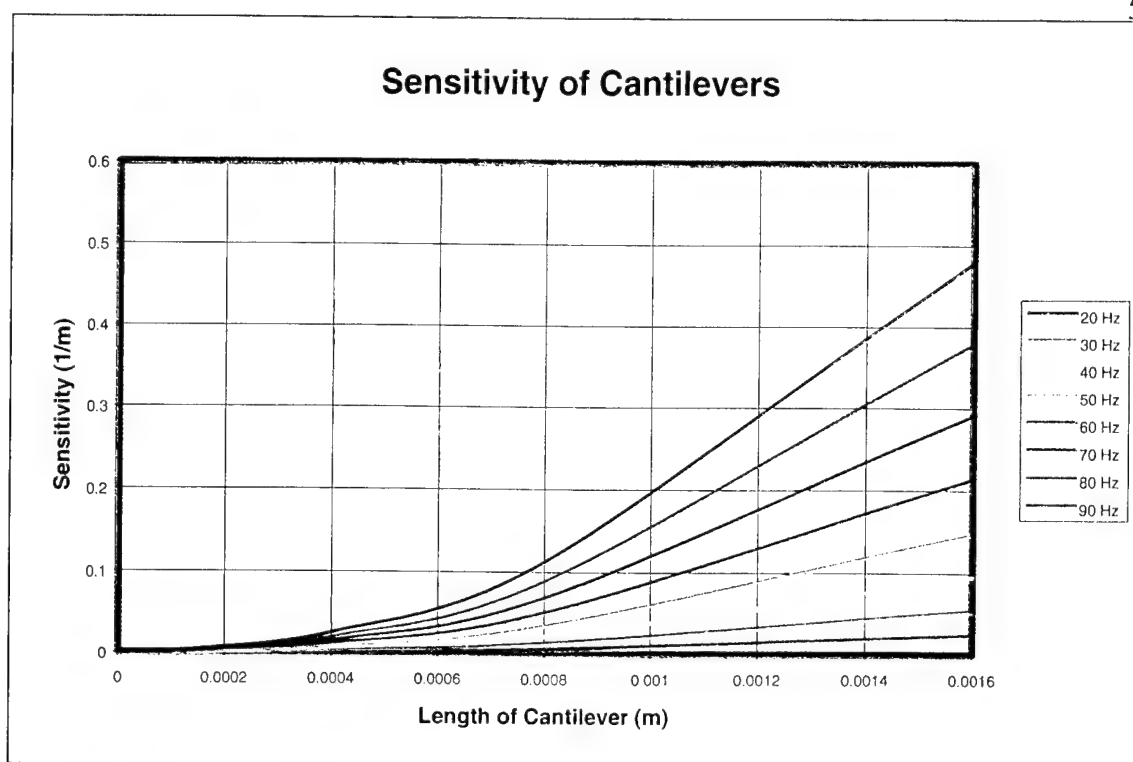


Figure 18: Sensitivity of Cantilevers

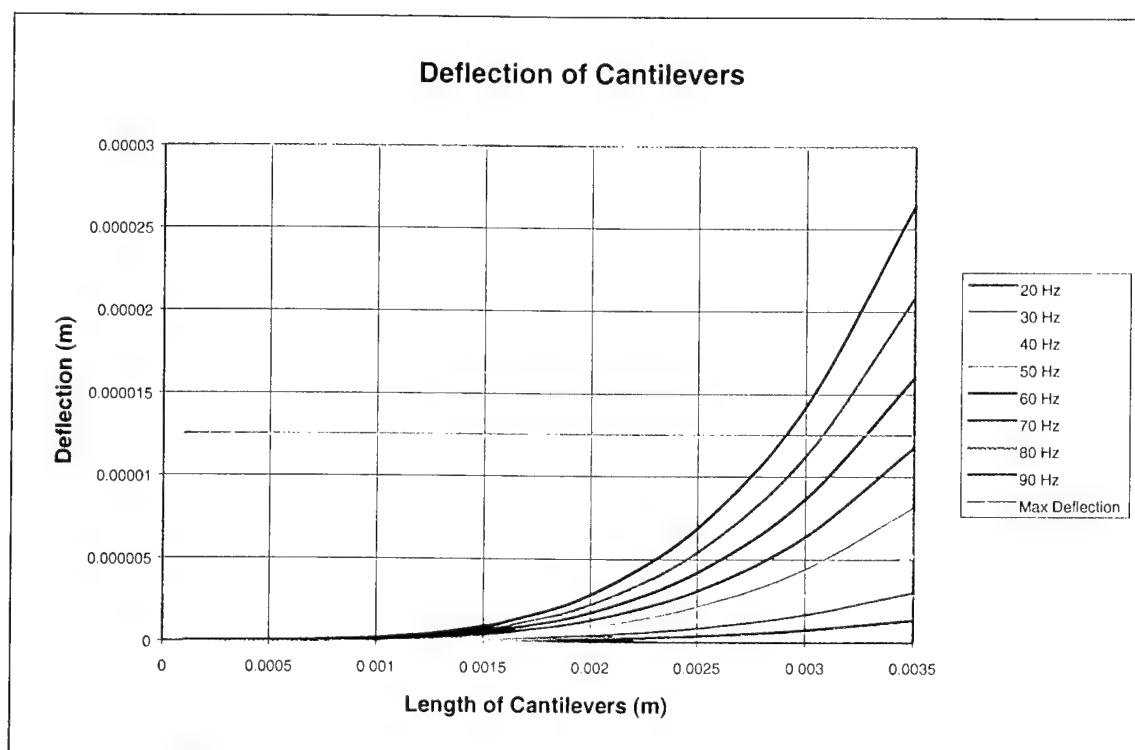


Figure 19: Deflection of Cantilevers

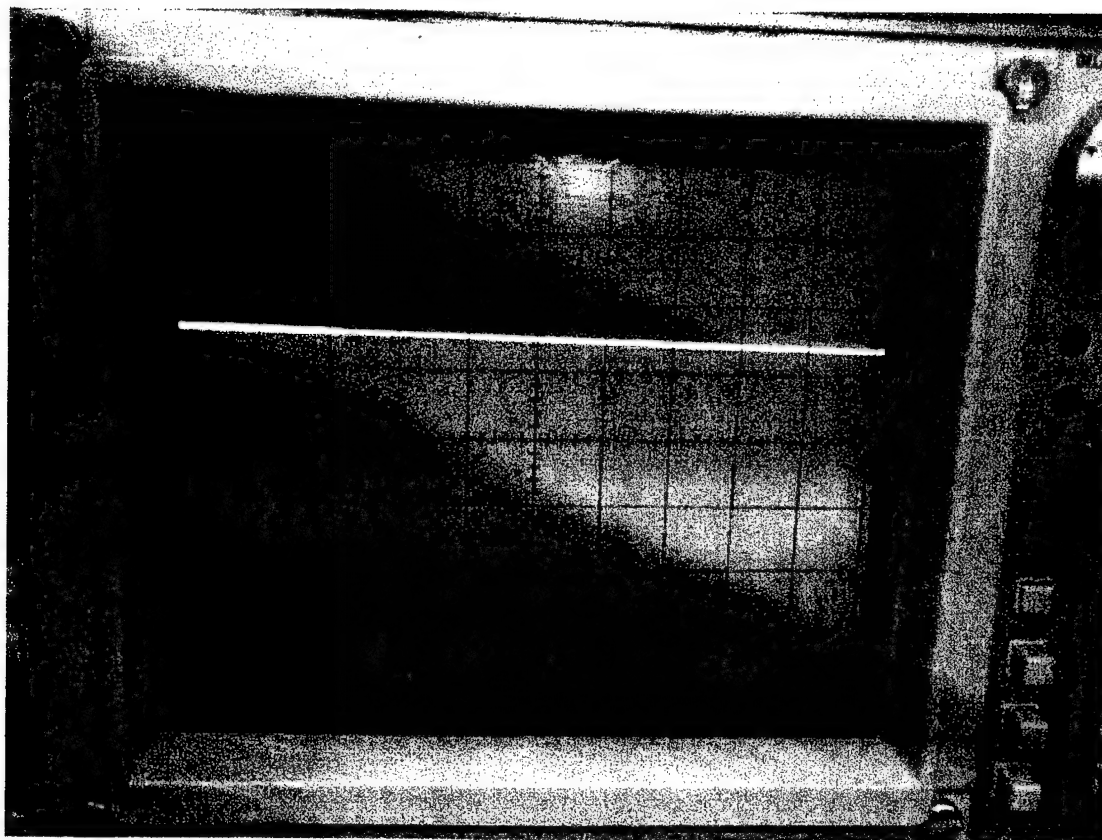


Figure 20: Noise Reading on Oscilloscope

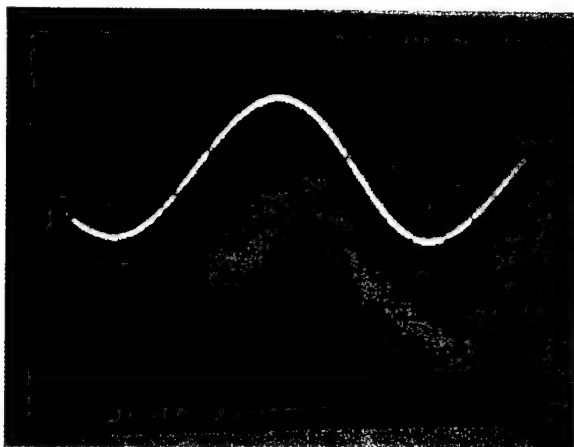


Figure 21a: Open Wires Signal

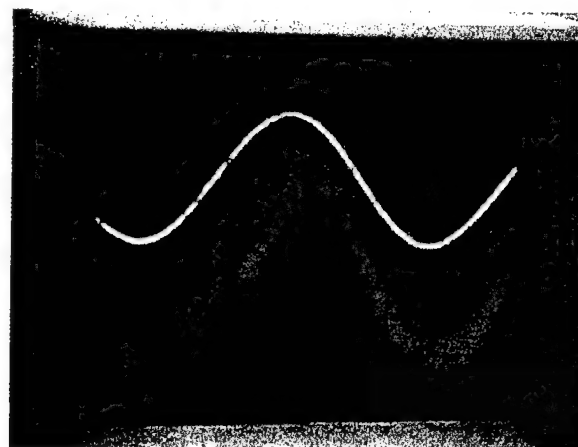


Figure 21c: Closed Wires Signal



Figure 21b: Experimental Set-up with
Open wires



Figure 21d: Experimental Set-up with
Closed wires

Figure 21: Noise Pick-up

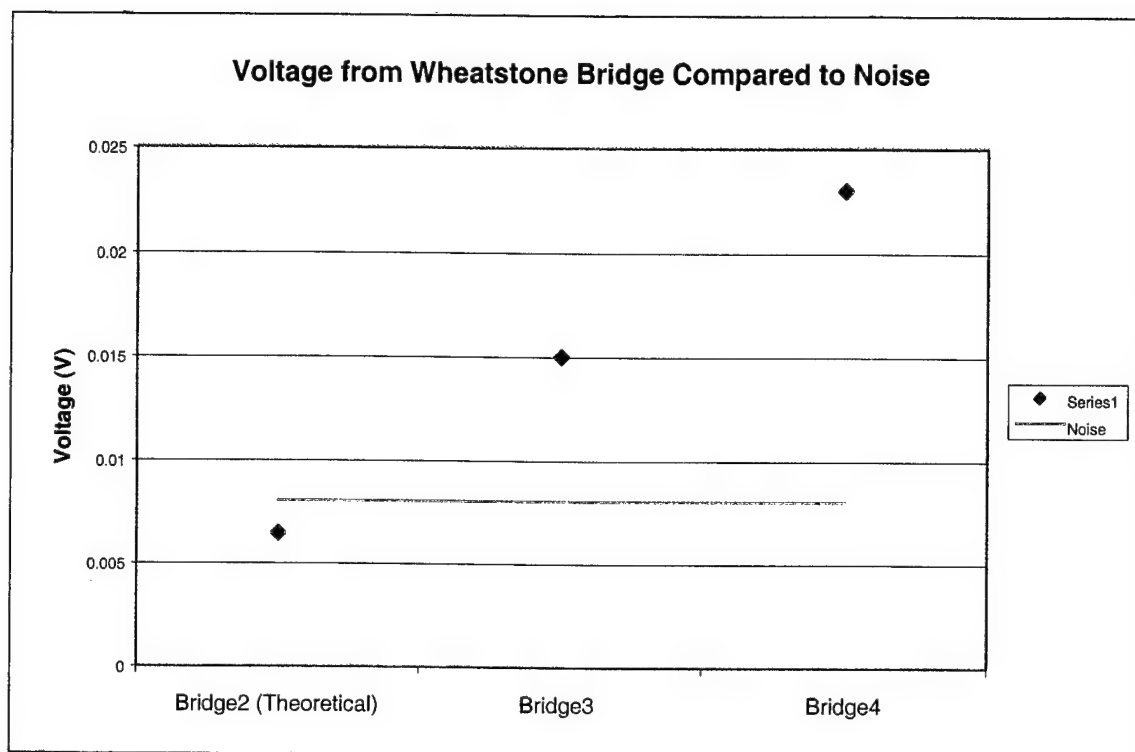


Figure 22: Voltage from Wheatstone Bridges Compared to Noise

Appendix A: Equations of Motion for Cantilever Used in Project

Equation 3-4 is the wave equation:

$$\frac{\partial^2 Y}{\partial t^2} = -\frac{EI}{mL^4} \frac{\partial^4 Y}{\partial u^4} = -\frac{1}{K^2} \frac{\partial^4 Y}{\partial u^4} \quad (3-4)$$

Use separation of variables to solve by assuming [Geist, 1997]:

$$Y = F(t) G(u) = \left[Y_o \sin(\omega t) \right] \left[1 + \frac{K^2 \omega^2 v(u)}{24} \right] \quad (A-1)$$

By imposing the boundary conditions defined by Equations 3-5 through 3-12 on Equation A-1 the solutions become:

$$Y_A(0, t) = \left[Y_o \sin(\omega t) \right] \left[1 + \frac{K_A^2 \omega^2 v_A(0)}{24} \right] = Y_o \sin(\omega t) \quad (A-2)$$

$$\therefore v_A(0) = 0$$

$$\frac{\partial Y_A}{\partial u}(0, t) = \left[Y_o \sin(\omega t) \right] \left[\frac{K_A^2 \omega^2 v'_A(0)}{24} \right] = 0 \quad (A-3)$$

$$\therefore v'_A(0) = 0$$

$$\frac{\partial^2 Y_B}{\partial u^2}(1, t) = \left[Y_o \sin(\omega t) \right] \left[\frac{K_B^2 \omega^2 v''_B(1)}{24} \right] = 0 \quad (A-4)$$

$$\therefore v''_B(1) = 0$$

$$\frac{\partial^3 Y_B}{\partial u^3}(1, t) = \left[Y_o \sin(\omega t) \right] \left[\frac{K_B^2 \omega^2 v'''_B(1)}{24} \right] = 0 \quad (A-5)$$

$$\therefore v'''_B(1) = 0$$

$$\left[y_o \sin(\omega t) \right] \left[\frac{K_A^2 \omega^2 v_A(\alpha)}{24} \right] = \left[y_o \sin(\omega t) \right] \left[\frac{K_B^2 \omega^2 v_B(\alpha)}{24} \right] \quad (A-6)$$

$$\therefore K_A^2 v_A(\alpha, t) = K_B^2 v_B(\alpha, t)$$

$$\left[y_o \sin(\omega t) \right] \left[\frac{K_A^2 \omega^2 v'_A(\alpha)}{24} \right] = \left[y_o \sin(\omega t) \right] \left[\frac{K_B^2 \omega^2 v'_B(\alpha)}{24} \right] \quad (A-7)$$

$$\therefore K_A^2 v'_A(\alpha, t) = K_B^2 v'_B(\alpha, t)$$

$$(EI)_A \left[y_o \sin(\omega t) \right] \left[\frac{K_A^2 \omega^2 v''_A(\alpha)}{24} \right] = (EI)_B \left[y_o \sin(\omega t) \right] \left[\frac{K_B^2 \omega^2 v''_B(\alpha)}{24} \right] \quad (A-8)$$

$$\therefore m_A v''_A(\alpha, t) = m_B v''_B(\alpha, t)$$

$$(EI)_A \left[y_o \sin(\omega t) \right] \left[\frac{K_A^2 \omega^2 v'''_A(\alpha)}{24} \right] = (EI)_B \left[y_o \sin(\omega t) \right] \left[\frac{K_B^2 \omega^2 v'''_B(\alpha)}{24} \right] \quad (A-9)$$

$$\therefore K_A^2 v'''_A(\alpha, t) = K_B^2 v'''_B(\alpha, t)$$

Assume that $v(u)$ is of the form for static deflection of a cantilever under uniform load [Riley, 1989]:

$$v(u) = 6Cu^2 - 4Du^3 + u^4 \quad (A-10)$$

Note that there is a $v_A(u)$ and $v_B(u)$ which represents each segment of the cantilever.

Now A-10 is used to evaluate the boundary conditions in order to determine D_A , C_A , D_B , and C_B . Equations A-2 and A-3 do not provide useful equations for the constants.

Apply Equation A-4 to A-10:

$$v_B'(1) = 12C_B - 24D_B + 12 = 0 \quad (A-11)$$

Apply Equation A-5 to A-10:

$$v_B'''(1) = -24D_B + 24 = 0 \quad (\text{A-12})$$

Solving A-11 and A-12 gives:

$$D_B = C_B = 1 \quad (\text{A-16})$$

Apply Equation A-6 to A-10:

$$K_A^2(6C_A\alpha^2 - 4D_A\alpha^3 + \alpha^4) = K_B^2(6\alpha^2 - 4\alpha^3 + \alpha^4) \quad (\text{A-17})$$

Apply Equation A-7 to A-10:

$$K_A^2(12C_A\alpha - 12D_A\alpha^2 + 4\alpha^3) = K_B^2(12\alpha - 12\alpha^2 + 4\alpha^3) \quad (\text{A-18})$$

Apply Equation A-8 to A-10:

$$m_A(12C_A - 24D_A\alpha + 12\alpha^2) = m_B(12 - 24\alpha + 12\alpha^2) \quad (\text{A-19})$$

Apply Equation A-9 to A-10:

$$m_A(-24D_A + 24\alpha) = m_B(-24 + 24\alpha) \quad (\text{A-20})$$

Solving Equation A-20 for D_A yields:

$$D_A = \frac{m_B}{m_A}(1 - \alpha) + \alpha \quad (\text{A-21})$$

Substituting A-21 into A-19 and solving for C_A gives:

$$C_A = \frac{m_B}{m_A}(1 - \alpha^2) + \alpha^2 \quad (\text{A-22})$$

By substituting the constants into $v_A(u)$, the equation for deflection of segment A evaluated at $u=\alpha$ becomes:

$$y(\alpha, t) = y_o \sin(\omega t) \left[1 + \frac{L^4 \omega^2 [2m_B(\alpha^2 - \alpha^3) + 3m_A \alpha^4]}{24 (EI)_A} \right] \quad (A-23)$$

Appendix B: Determination of Strain in Piezoresistive Layer (Refer to Figure 7)

This appendix was done in accordance with Geist [1997].

The distance, ds' , is determined from the Pythagorean theorem as:

$$ds' = \sqrt{dx^2 + dy^2} \quad (B-1)$$

If the slope of the beam is assumed to be small, i.e.,

$$\frac{dy}{dx} \ll 1 \quad (B-2)$$

then the square of the slope can be neglected :

$$ds' = dx \sqrt{1 + \left(\frac{dy}{dx}\right)^2} \approx dx \quad (B-3)$$

The length, $L_{NPP}(t)$, of the neutral plane of the piezoresistive layer is found by relating ds to ds' through the use of similar triangles. The resulting ratio is:

$$\frac{ds}{ds'} = \frac{r(x,t) + h}{r(x,t)} \quad (B-4)$$

Use Equations B-3 and B-4 to get:

$$L_{NPP}(t) = \int_0^c ds = \int_0^c \frac{r(x,t) + h}{r(x,t)} dx \quad (B-5)$$

The slope of the beam is related to the radius of curvature of a circle by the relationship:

$$r(x, t) = \frac{\left(1 + \left[\frac{\partial Y(x, t)}{\partial x}\right]^2\right)^{\frac{3}{2}}}{\frac{\partial^2 Y(x, t)}{\partial x^2}} \quad (\text{B-6})$$

Using Equation B-2, Equation B-6 simplifies to:

$$r(x, t) \approx \frac{1}{\frac{\partial^2 Y(x, t)}{\partial x^2}} \quad (\text{B-7})$$

By substituting Equation B-7 into Equation B-5 the equation becomes:

$$L_{\text{NPP}}(t) = \int_0^c \left(1 + \frac{\partial^2 Y(x, t)}{\partial x^2} h\right) dx = x + \frac{\partial Y(x, t)}{\partial x} \Big|_0^c h = c + h \frac{\partial Y(c, t)}{\partial x} - 0 - \frac{\partial Y(0, t)}{\partial x} \quad (\text{B-8})$$

Boundary condition found in Equation 3-3 is applied to Equation B-8 giving:

$$L_{\text{NPP}}(t) = c + h \frac{\partial Y(c, t)}{\partial x} \quad (\text{B-9})$$

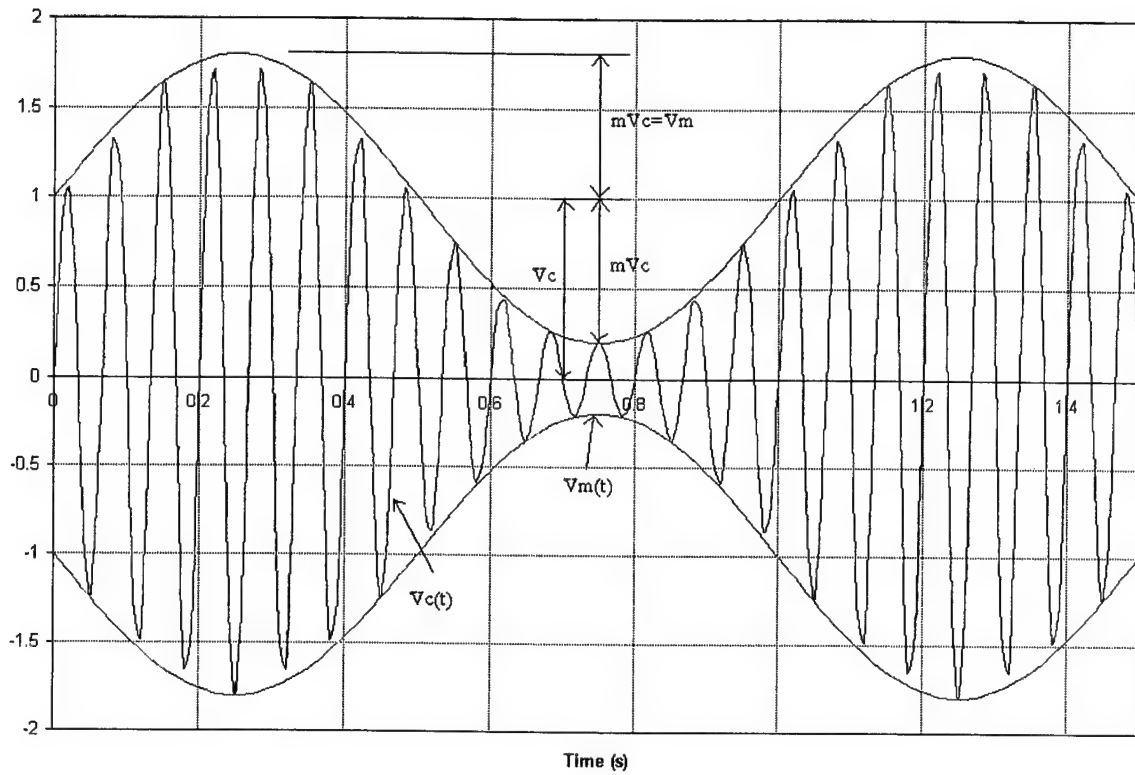
The definition of strain is then applied and the differential change in the length of the neutral plane of the piezoresistor is given by:

$$\frac{L_{NPP}(t) - L_{NPP}(0)}{L_{NPP}(0)} = \frac{c + h \frac{\partial y(c, t)}{\partial x} - c}{c} = \frac{h}{c} \frac{\partial y(c, t)}{\partial x} \quad (B-10)$$

Non-dimensionalizing the length with $u=x/L$ ($\alpha=c/L$), Equation B-10 becomes:

$$\frac{L_{NPP}(t) - L_{NPP}(0)}{L_{NPP}(0)} = \frac{h}{\alpha L^2} \frac{\partial y(\alpha, t)}{\partial u} \quad (B-11)$$

Appendix C: Determination of Instantaneous Resistance in Terms of Piezoresistive Sensitivity



In amplitude modulation (AM) information is superimposed on a carrier signal. The carrier $V_c(t) = V_c \sin(\omega_c t)$ is varied by the modulating signal $V_m(t) = V_m \sin(\omega_m t)$. The equation of the amplitude-modulated wave is

$$V_{AM} = (1 + m \sin(\omega_m t)) V_c \sin(\omega_c t) \quad (C-1)$$

where m is the degree of modulation defined by

$$m = \frac{V_m}{V_c} = \frac{V_{\max} - V_{\min}}{V_{\max} + V_{\min}} \quad (C-2)$$

where

$$V_c = \frac{V_{\max} + V_{\min}}{2} \quad (C-3)$$

$$V_m = \frac{V_{\max} - V_{\min}}{2} \quad (C-4)$$

In the experimental set-up, DC current means that voltage and resistance are directly proportional according to Ohm's law. Therefore, the carrier can be represented by $R_c(t) = R_c \sin(\omega_c t)$ and the modulating signal by $R_m(t) = R_m \sin(\omega_m t)$. The equation of the amplitude modulation then becomes:

$$R(t) = (1 + m \sin(\omega_m t)) R_c \sin(\omega_c t) \quad (C-5)$$

where

$$m = \frac{R_m}{R_c} = \frac{R_{\max} - R_{\min}}{R_{\max} + R_{\min}} \quad (C-6)$$

Because the carrier voltage has a DC current and not an AC current Equation C-5 simplifies to

$$R(t) = (1 + m \sin(\omega_m t)) R_c \quad (C-7)$$

Piezoresistive sensitivity, S , relates the change in the resistance of an encapsulated piezoresistor to the amplitude, y_o , of a sinusoidal vibration driving the base of a cantilever structure. The definition of piezoresistive sensitivity is [Brand, 1994]:

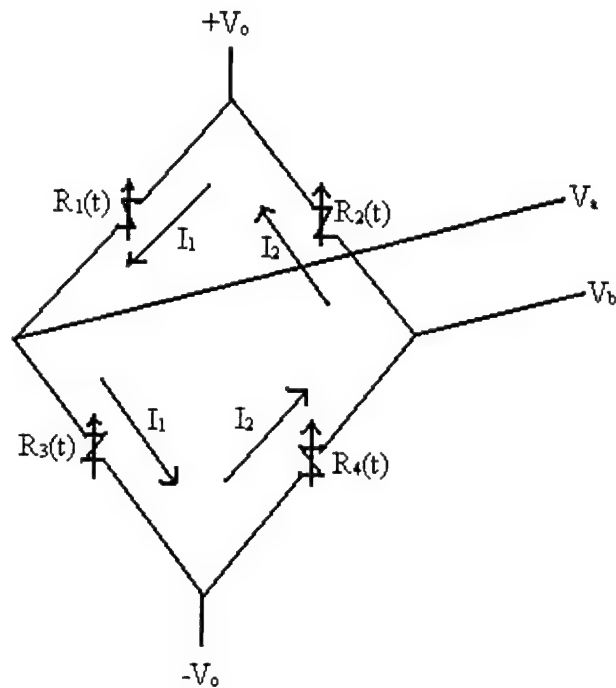
$$Sy_o = \frac{R_{\max} - R_{\min}}{R_{\max} + R_{\min}} \quad (C-8)$$

By comparing Equations C-7 and C-8 it is seen that $m=Sy_o$. Substituting this back into C-7 gives an expression which relates instantaneous resistance to piezoresistive vibration sensitivity:

$$R(t) = (1 + Sy_o \sin(\omega_m t)) R_c \quad (C-9)$$

Appendix D: Relating the Piezoresistive Sensitivity to Experimental Results

A diagram of a Wheatstone bridge made of four different variable resistors is seen below:



The currents through the branches of the Wheatstone bridge are I_1 and I_2 . The currents are determined by using Ohm's law and two equivalent terms are developed using currents I_1 and I_2 for each branch of the Wheatstone bridge.

$$I_1 = \frac{V_o - V_a}{R_1(t)} = \frac{V_a - (-V_o)}{R_3(t)} \quad (D-1)$$

$$I_2 = \frac{-V_o - V_b}{R_4(t)} = \frac{V_b - V_o}{R_2(t)} \quad (D-2)$$

By eliminating the currents and solving for V_a and V_b the equations become:

$$V_a = \frac{V_o (R_3(t) - R_1(t))}{R_1(t) + R_3(t)} \quad (D-3) \quad V_b = \frac{V_o (R_4(t) - R_2(t))}{R_2(t) + R_4(t)}$$

(D-4)

The voltage across the Wheatstone bridge, ΔV , is the difference of V_a and V_b . By using Equations 3 and 4, the voltage, ΔV , becomes:

$$\Delta V = V_a - V_b = V_o \left(\frac{R_3(t) - R_1(t)}{R_1(t) + R_3(t)} - \frac{R_4(t) - R_2(t)}{R_2(t) + R_4(t)} \right) \quad (D-5)$$

The values of instantaneous resistance of each of the cantilevers in the Wheatstone bridge are seen below:

$$R_1(t) = R(0) (1 + \Delta_1) \quad (D-6)$$

$$R_2(t) = R(0) (1 + \Delta_2) \quad (D-7)$$

$$R_3(t) = R(0) (1 + \Delta_3) \quad (D-8)$$

$$R_4(t) = R(0) (1 + \Delta_4) \quad (D-9)$$

where

$$\Delta_n = S_n y_o \sin(\omega t)$$

for $n=1,2,3,4$

The piezoresistive sensitivity, S , is defined in Equation 3-21 of the report where S is different for each length cantilever.

By substituting Equations D-6 through D-9 into Equation D-5, the value of ΔV becomes

$$\Delta V = \frac{2V_o R(0) (1 + \Delta_3)}{R(0) (2 + \Delta_1 + \Delta_3)} - \frac{2V_o R(0) (1 + \Delta_4)}{R(0) (2 + \Delta_2 + \Delta_4)} \quad (D-10)$$

Below Equation D-10 is put into expanded form:

$$\Delta V = \frac{2V_o \left[(1 + \Delta_3) (2 + \Delta_2 + \Delta_4) - (1 + \Delta_4) (2 + \Delta_1 + \Delta_3) \right]}{(2 + \Delta_1 + \Delta_3) (2 + \Delta_2 + \Delta_4)}$$

$$\Delta V = \frac{2V_o \left[2 + \Delta_2 + \Delta_4 + 2\Delta_3 + \Delta_3(\Delta_2 + \Delta_4) - 2 - \Delta_1 - \Delta_3 - 2\Delta_4 - \Delta_4(\Delta_1 + \Delta_3) \right]}{4 + 2(\Delta_1 + \Delta_2 + \Delta_3 + \Delta_4) + (\Delta_1 + \Delta_3)(\Delta_2 + \Delta_4)}$$

With the assumption for $\Delta_n \ll 1$, the terms $\Delta_i \Delta_j$ drop out and the expanded form of Equation 10 simplifies to:

$$\Delta V \approx \frac{V_o [\Delta_2 + \Delta_3 - \Delta_1 - \Delta_4]}{2} = \frac{V_o [S_2 + S_3 - S_1 - S_4] Y_o \sin(\omega t)}{2} \quad (D-11)$$

The maximum change in voltage occurs when $\sin(\omega t)=1$ and the minimum change in

voltage occurs when $\sin(\omega t) = -1$. The maximum and minimum changes in voltage become

$$\Delta V_{\max} = -\Delta V_{\min} = \frac{V_o Y_o [S_2 + S_3 - S_1 - S_4]}{2} \quad (\text{D-12})$$

The difference of the maximum and minimum change in voltage is

$$\Delta V_{\max} - \Delta V_{\min} = V_o Y_o [S_2 + S_3 - S_1 - S_4] \quad (\text{D-13})$$

Appendix E: Determination of Beam Properties

Material Properties:

Polysilicon:

$$E_p := 150 \cdot 10^9 \text{ Pa}$$

$$\nu_p := 0.17$$

$$\rho_p := 2300 \frac{\text{kg}}{\text{m}^3}$$

Silicon Oxide:

$$E_s := 70 \cdot 10^9 \text{ Pa}$$

$$\nu_s := 0.17$$

$$\rho_s := 2200 \frac{\text{kg}}{\text{m}^3}$$

Air:

$$E_a := 0 \text{ Pa}$$

$$\rho_a := 1.184 \frac{\text{kg}}{\text{m}^3}$$

Assume isotropic material

$$E_{pxx} := \frac{E_p}{(1 - \nu_p^2)}$$

$$E_{pxx} = 1.545 \cdot 10^{11} \text{ Pa}$$

$$E_{sxx} := \frac{E_s}{(1 - \nu_s^2)}$$

$$E_{sxx} = 7.208 \cdot 10^{10} \text{ Pa}$$

Segment "A"

The beam has 2 materials (Silicon Oxide and Polysilicon) in segment "A":

The beam has 4 physical layers in segment "A":

Physical Layer 1:

Flexural Rigidity:

$$EI1 := \int_0^{0.6 \cdot 10^{-6}} \int_0^{25 \cdot 10^{-6}} E_{sxx} y^2 dx dy$$

$$EI1 = 1.297 \cdot 10^{-13} \frac{\text{kg} \cdot \text{m}^3}{\text{s}^2}$$

Mass per Unit Length:

$$m1 := \int_0^{0.6 \cdot 10^{-6}} \int_0^{25 \cdot 10^{-6}} \rho_s dx dy$$

$$m1 = 3.3 \cdot 10^{-8} \frac{\text{kg}}{\text{m}}$$

Physical Layer 2:

Flexural Rigidity:

$$a := \int_{0.6 \cdot 10^{-6}}^{1 \cdot 10^{-6}} \int_0^{10 \cdot 10^{-6}} E s x x y^2 dx dy \quad d := \int_{0.6 \cdot 10^{-6}}^{1 \cdot 10^{-6}} \int_{13 \cdot 10^{-6}}^{15 \cdot 10^{-6}} E p x x y^2 dx dy$$

$$b := \int_{0.6 \cdot 10^{-6}}^{1 \cdot 10^{-6}} \int_{10 \cdot 10^{-6}}^{12 \cdot 10^{-6}} E p x x y^2 dx dy \quad e := \int_{0.6 \cdot 10^{-6}}^{1 \cdot 10^{-6}} \int_{15 \cdot 10^{-6}}^{25 \cdot 10^{-6}} E s x x y^2 dx dy$$

$$c := \int_{0.6 \cdot 10^{-6}}^{1 \cdot 10^{-6}} \int_{12 \cdot 10^{-6}}^{13 \cdot 10^{-6}} E s x x y^2 dx dy$$

$$a = 1.884 \cdot 10^{-13}$$

$$c = 1.884 \cdot 10^{-14}$$

$$e = 1.884 \cdot 10^{-13}$$

$$b = 8.073 \cdot 10^{-14}$$

$$d = 8.073 \cdot 10^{-14}$$

$$EI2 := a + b + c + d + e$$

$$EI2 = 5.571 \cdot 10^{-13} \quad \frac{\text{kg} \cdot \text{m}^3}{\text{s}^2}$$

Mass per Unit Length:

$$f := \int_{0.6 \cdot 10^{-6}}^{1 \cdot 10^{-6}} \int_0^{10 \cdot 10^{-6}} \rho s dx dy \quad i := \int_{0.6 \cdot 10^{-6}}^{1 \cdot 10^{-6}} \int_{13 \cdot 10^{-6}}^{15 \cdot 10^{-6}} \rho p dx dy$$

$$g := \int_{0.6 \cdot 10^{-6}}^{1 \cdot 10^{-6}} \int_{10 \cdot 10^{-6}}^{12 \cdot 10^{-6}} \rho p dx dy \quad j := \int_{0.6 \cdot 10^{-6}}^{1 \cdot 10^{-6}} \int_{15 \cdot 10^{-6}}^{25 \cdot 10^{-6}} \rho s dx dy$$

$$h := \int_{0.6 \cdot 10^{-6}}^{1 \cdot 10^{-6}} \int_{12 \cdot 10^{-6}}^{13 \cdot 10^{-6}} \rho s dx dy$$

$$f = 8.8 \cdot 10^{-9}$$

$$h = 8.8 \cdot 10^{-10}$$

$$j = 8.8 \cdot 10^{-9}$$

$$g = 1.84 \cdot 10^{-9}$$

$$i = 1.84 \cdot 10^{-9}$$

$$m2 := f + g + h + i + j$$

$$m2 = 2.216 \cdot 10^{-8} \quad \frac{\text{kg}}{\text{m}}$$

Physical Layer 3:

Flexural Rigidity:

Mass per Unit Length:

$$EI3 := \int_{1 \cdot 10^{-6}}^{3.7 \cdot 10^{-6}} \int_0^{25 \cdot 10^{-6}} Esxy^2 dx dy \quad m3 := \int_{1 \cdot 10^{-6}}^{3.7 \cdot 10^{-6}} \int_0^{25 \cdot 10^{-6}} \rho s dx dy$$

$$EI3 = 2.983 \cdot 10^{-11} \quad \frac{\text{kg} \cdot \text{m}^3}{\text{s}^2} \quad m3 = 1.485 \cdot 10^{-7} \quad \frac{\text{kg}}{\text{m}}$$

Physical Layer 4:

Flexural Rigidity:

$$k := \int_{3.7 \cdot 10^{-6}}^{4.1 \cdot 10^{-6}} \int_0^{6.9 \cdot 10^{-6}} Ea \cdot y^2 dx dy \quad m := \int_{3.7 \cdot 10^{-6}}^{4.1 \cdot 10^{-6}} \int_{21.9 \cdot 10^{-6}}^{25 \cdot 10^{-6}} Ea \cdot y^2 dx dy$$

$$l := \int_{3.7 \cdot 10^{-6}}^{4.1 \cdot 10^{-6}} \int_{6.9 \cdot 10^{-6}}^{21.9 \cdot 10^{-6}} Esxy^2 dx dy \quad k = 0$$

$$l = 6.584 \cdot 10^{-12} \quad m = 0$$

$$EI4 := k + l + m$$

$$EI4 = 6.584 \cdot 10^{-12} \quad \frac{\text{kg} \cdot \text{m}^3}{\text{s}^2}$$

Mass per Unit Length:

$$n := \int_{3.7 \cdot 10^{-6}}^{4.1 \cdot 10^{-6}} \int_0^{6.9 \cdot 10^{-6}} \rho a dx dy \quad p := \int_{3.7 \cdot 10^{-6}}^{4.1 \cdot 10^{-6}} \int_{21.9 \cdot 10^{-6}}^{25 \cdot 10^{-6}} \rho a dx dy$$

$$o := \int_{3.7 \cdot 10^{-6}}^{4.1 \cdot 10^{-6}} \int_{6.9 \cdot 10^{-6}}^{21.9 \cdot 10^{-6}} \rho s dx dy \quad n = 3.268 \cdot 10^{-12}$$

$$o = 1.32 \cdot 10^{-8}$$

$$p = 1.468 \cdot 10^{-12}$$

$$m4 := n + o + p$$

$$m4 = 1.32 \cdot 10^{-8} \quad \frac{\text{kg}}{\text{m}}$$

Segment "B"

The beam has 1 material in segment "B"

The beam has 2 physical layers in segment "B":

Physical Layer 1:

Flexural Rigidity:

Mass per Unit Length:

$$EI1b := \int_0^{3.7 \cdot 10^{-6}} \int_0^{25 \cdot 10^{-6}} E_{sxx} y^2 dx dy \quad m1b := \int_0^{3.7 \cdot 10^{-6}} \int_0^{25 \cdot 10^{-6}} \rho_s dx dy$$

$$EI1b = 3.043 \cdot 10^{-11} \quad \frac{\text{kg} \cdot \text{m}^3}{\text{s}^2} \quad m1b = 2.035 \cdot 10^{-7} \quad \frac{\text{kg}}{\text{m}}$$

Physical Layer 2:

Flexural Rigidity:

$$k := \int_{3.7 \cdot 10^{-6}}^{4.1 \cdot 10^{-6}} \int_0^{6.9 \cdot 10^{-6}} E_a y^2 dx dy \quad m := \int_{3.7 \cdot 10^{-6}}^{4.1 \cdot 10^{-6}} \int_{21.9 \cdot 10^{-6}}^{25 \cdot 10^{-6}} E_a y^2 dx dy$$

$$l := \int_{3.7 \cdot 10^{-6}}^{4.1 \cdot 10^{-6}} \int_{6.9 \cdot 10^{-6}}^{21.9 \cdot 10^{-6}} E_{sxx} y^2 dx dy \quad k = 0$$

$$l = 6.584 \cdot 10^{-12}$$

$$m = 0$$

$$EI2b := k + l + m$$

$$EI2b = 6.584 \cdot 10^{-12} \quad \frac{\text{kg} \cdot \text{m}^3}{\text{s}^2}$$

Mass per Unit Length:

$$n := \int_{3.7 \cdot 10^{-6}}^{4.1 \cdot 10^{-6}} \int_0^{6.9 \cdot 10^{-6}} \rho_a dx dy \quad p := \int_{3.7 \cdot 10^{-6}}^{4.1 \cdot 10^{-6}} \int_{21.9 \cdot 10^{-6}}^{25 \cdot 10^{-6}} \rho_a dx dy$$

$$o := \int_{3.7 \cdot 10^{-6}}^{4.1 \cdot 10^{-6}} \int_{6.9 \cdot 10^{-6}}^{21.9 \cdot 10^{-6}} \rho_s dx dy \quad n = 3.268 \cdot 10^{-12}$$

$$o = 1.32 \cdot 10^{-8}$$

$$p = 1.468 \cdot 10^{-12}$$

$$m2b := n + o + p$$

$$m2b = 1.32 \cdot 10^{-8} \quad \frac{\text{kg}}{\text{m}}$$

Properties of Beam:Properties of Segment "A":

Flexural Rigidity of Segment "A":

$$EI_A := EI1 + EI2 + EI3 + EI4$$

$$EI_A = 3.71 \cdot 10^{-11} \quad \frac{\text{kg} \cdot \text{m}^3}{\text{s}^2}$$

Mass per Unit Length of Segment "A":

$$m_A := m1 + m2 + m3 + m4$$

$$m_A = 2.169 \cdot 10^{-7} \quad \frac{\text{kg}}{\text{m}}$$

Properties of Segment "B":

Flexural Rigidity of Segment "B":

$$EI_B := EI1b + EI2b$$

$$EI_B = 3.701 \cdot 10^{-11} \quad \frac{\text{kg} \cdot \text{m}}{\text{s}^2}$$

Mass per Unit Length of Segment "B":

$$m_B := m1b + m2b$$

$$m_B = 2.167 \cdot 10^{-7} \quad \frac{\text{kg}}{\text{m}}$$

Appendix F: Calculation of Distance, h, Between NPP and NPB

Use Figure 5 for measurements of beam.

With the use of first moment of Area and a common axis of $y=2.35$
the distance of the NPB was determined in reference to the common axis.

$$A \cdot y' := \left(11.2 \mu\text{m} \cdot 0.4 \mu\text{m} + 25 \mu\text{m} \cdot 2.7 \mu\text{m} + 21 \mu\text{m} \cdot 0.4 \mu\text{m} + \frac{150}{70} \cdot 4 \mu\text{m} \cdot 0.4 \mu\text{m} + 25 \mu\text{m} \cdot 0.6 \mu\text{m} \right) \cdot y'$$

$$A \cdot y' := \left(11.2 \mu\text{m} \cdot 0.4 \mu\text{m} \cdot 1.55 \mu\text{m} - 21 \mu\text{m} \cdot 0.4 \mu\text{m} \cdot 1.55 \mu\text{m} - \frac{150}{70} \cdot 4 \mu\text{m} \cdot 0.4 \mu\text{m} \cdot 1.55 \mu\text{m} - 25 \mu\text{m} \cdot 0.6 \mu\text{m} \cdot 2.05 \mu\text{m} \right)$$

$$98.809 \cdot 10^{-12} \cdot y' := -42.1403 \cdot 10^{-18}$$

$$y' := -.42648 \mu\text{m}$$

$$\text{NPB} := 2.35 \mu\text{m} - .42684 \mu\text{m}$$

$$\text{NPB} := 1.9235 \mu\text{m}$$

The location of the NPP=0.8 μm , which bisects the piezoresistor.

$$h := \text{NPB} - \text{NPP}$$

$$h := 1.1235 \mu\text{m}$$

Appendix G: Sample Calculation of Z for Package1

	From Appendix E:	From Appendix F:
<u>Length of beam</u>	<u>Mass per Unit Length</u>	$h := 1.1235 \cdot 10^{-6} \text{ m}$
$L := 0.8 \cdot 10^{-3} \text{ m}$	$m_A := 2.169 \cdot 10^{-7} \frac{\text{kg}}{\text{m}}$	
<u>Length of Piezoresistor</u>	$m_B := 2.167 \cdot 10^{-7} \frac{\text{kg}}{\text{m}}$	
$c := 0.1 \cdot 10^{-3} \text{ m}$	<u>Flexural Rigidity</u>	
<u>Gain of Amplifier</u>	$EI_A := 3.71 \cdot 10^{-11} \frac{\text{kg} \cdot \text{m}^3}{\text{s}^2}$	
$G := 42.78$		
<u>max acceleration</u>		
$\omega^2 \cdot y_o := 144.06 \frac{\text{m}}{\text{s}^2}$		

$$\Delta V_{\max} - \Delta V_{\min} := V_o \cdot y_o \cdot (S_1 + S_2 - S_3 - S_4)$$

Package1 contains Bridge3 which has two 0.8 mm cantilevers and two reference cantilev

Because the Wheatstone bridge used contains 2 reference cantilevers:

$$S_3 = S_4 = 0$$

Because the Wheatstone bridge has two 0.8 mm cantilevers:

$$S_1 = S_2$$

The volatge from the Bridge had a gain, G, from the amplifier

Thus

$$\frac{\Delta V_{\max} - \Delta V_{\min}}{G} := V_o \cdot y_o \cdot 2 \cdot S_1$$

where

$$S_1 := \frac{\left[Z L^2 \cdot \omega^2 \cdot h \cdot \left[3 \cdot m_B \cdot \left[1 - \left(\frac{c}{L} \right) \right] + m_A \cdot \left(\frac{c}{L} \right)^2 \right] \right]}{6 \cdot EI_A}$$

$$\frac{\Delta V_{\max} - \Delta V_{\min}}{G} := \frac{V_o \cdot y_o \cdot 2 \cdot Z \cdot L^2 \cdot \omega^2 \cdot h \cdot \left[3 \cdot m_B \cdot \left[1 - \left(\frac{c}{L} \right) \right] + m_A \cdot \left(\frac{c}{L} \right)^2 \right]}{6 \cdot EI_A}$$

Solving for Z gives:

$$Z := 130$$

Appendix H: Sample Calculation of Piezoresistive Sensitivity

Length of Cantilever

Frequency

$$L := 0.8 \cdot 10^{-3} \quad \text{m}$$

$$\omega := 70 \cdot 2 \cdot \pi$$

Length of Piezoresistor

$$c := 0.1 \cdot 10^{-3} \quad \text{m}$$

From Appendix E:

From Appendix F:

From Report:

Mass per Unit Length

Distance from NPP to NPB

Piezoresistive Coefficient

$$m_A := 2.169 \cdot 10^{-7} \frac{\text{kg}}{\text{m}}$$

$$h := 1.1235 \cdot 10^{-6} \quad \text{m}$$

$$Z := 190$$

$$m_B := 2.167 \cdot 10^{-7} \frac{\text{kg}}{\text{m}}$$

Flexural Rigidity

$$EI_A := 3.71 \cdot 10^{-11}$$

Piezoresistive Sensitivity

$$S := \frac{\left[Z \cdot L^2 \cdot \omega^2 \cdot h \cdot \left[3 \cdot m_B \cdot \left(1 - \frac{c}{L} \right) + m_A \cdot \left(\frac{c}{L} \right)^2 \right] \right]}{6 \cdot EI_A}$$

$$S = 0.068 \quad \frac{1}{\text{m}}$$

Appendix I: Sample Calculation of Deflection

<u>Length of Beam</u>	<u>Frequency</u>	<u>Amplitude</u>
$L := 0.8 \cdot 10^{-3} \text{ m}$	$\omega := 60 \cdot 2 \pi \frac{\text{rad}}{\text{sec}}$	$y_0 := .00075 \text{ m}$

From Appendix E:

Flexural Rigidity

$$EI_B := 3.701 \cdot 10^{-11} \frac{\text{kg} \cdot \text{m}^3}{\text{s}^2}$$

Mass per Unit Length

$$m_B := 2.167 \cdot 10^{-7} \frac{\text{kg}}{\text{m}}$$

Deflection

$$y := y_0 \cdot \left(\frac{L^4 \cdot \omega^2 \cdot 3 \cdot m_B}{24 \cdot EI_B} \right)$$

$$y = 3.1954593 \cdot 10^{-8} \text{ m}$$